Industrial Chemistry & Materials

REVIEW

Check for updates

Recent progress of manganese dioxide based electrocatalysts for the oxygen evolution reaction

Yunlong He,[a] Zhenye Kang, [iD]*[a] Jing Li,[a] Yawei Li [iD]*[b] and Xinlong Tian [iD]*[a]

The oxygen evolution reaction (OER) represents an anodic reaction for a variety of sustainable energy conversion and storage technologies, such as hydrogen production, CO_2 reduction, *etc*. To realize the large-scale implementation of these technologies, the sluggish kinetics of the OER resulting from multi-step proton/electron transfer and occurring at the gas–liquid–solid triple-phase boundary needs to be accelerated. Manganese oxide-based (MnO_x) materials, especially MnO_2, have become promising non-precious metal electrocatalysts for the OER under acidic conditions due to the good trade-off between catalytic activity and stability. This paper reviews the recent progress of MnO_2-based materials to catalyze the OER through either the traditional adsorbent formation mechanism (AEM) or the emerging lattice-oxygen-mediated mechanism (LOM). Pure manganese dioxide OER catalysts with different crystalline structures and morphologies are summarized, while MnO_2-based composite structures are also discussed, and the application of MnO_2-based catalysts in PEMWEs is summarized. Critical challenges and future research directions are presented to hopefully help future research.

Keywords: Manganese dioxides; Electrocatalysts; Oxygen evolution reaction; Adsorbate evolution mechanism; Lattice-oxygen-mediated mechanism.

[a] State Key Laboratory of Marine Resource Utilization in South China Sea, Hainan Provincial Key Lab of Fine Chemistry, School of Chemical Engineering and Technology, Hainan University, Haikou 570228, China.
E-mail: zkang@hainanu.edu.cn, tianxl@hainanu.edu.cn
[b] School of Chemistry and Chemical Engineering, Shanxi University, Taiyuan 030006, China. E-mail: yaweili@sxu.edu.cn

1 Introduction

With the global warming problem caused by the consumption of traditional fossil fuels and the increase in carbon dioxide emissions, researchers worldwide have paid more attention to clean and sustainable energy sectors for decarbonization.[1–4] Increasing the share of intermittent and fluctuating renewable energy in the sustainable energy portfolio requires large-scale development and deployment of energy conversion and storage

Yunlong He is currently studying for his Master's degree at Hainan University, in the group of Prof. Zhenye Kang. His research mainly focuses on the application of manganese dioxide supported noble metal catalysts to the acid OER and PEMWEs.

Yunlong He

Zhenye Kang, Professor of Chemical Engineering and Technology College of Hainan University, Master/Doctoral Supervisor, received his PhD degree from the University of Tennessee (UTK) in 2018. He conducted his postdoctoral research at the U.S. Department of Energy's (DOE) National Laboratory for Renewable Energy (NREL) from 2018 to 2021. Then he joined the School of Chemical Engineering and Technology of Hainan University. His main research interests are the proton exchange membrane hydrolysis pool and fuel cell technology.

Zhenye Kang

solutions.[5–9] Hydrogen production *via* electrolytic water splitting coupled with renewable energies offers a promising candidate to fulfill the sustainable clean energy cycle, which can store the excess electricity energy into hydrogen and then release the energy in variable ways, such as fuel cells or combustion. However, the adoption of high noble metal loadings of platinum group metals, such as iridium or ruthenium, in water electrolysis devices for electrochemical reactions hinders wide commercialization. Specifically, the lack of high-performing and stable electrocatalysts for the oxygen evolution reaction (OER) is the main bottleneck in the large-scale production of green hydrogen.[10–16]

For electrolytic water, the hydrogen evolution reaction (HER) at the cathode occurs relatively easily. However, the OER at the anode involves four electron transfers, which is a complex multi-step and inherently slow kinetic process.[17–20] During the OER, oxygen molecules are produced by multiple electron/proton coupling processes, and the reaction is highly dependent on the pH value. The half-cell reaction of the OER can occur in alkaline media following: $4OH^- \leftrightarrow 2H_2O + O_2 + 4e^-$, and in acidic media following: $2H_2O \leftrightarrow 4H^+ + O_2 + 4e^-$.[21–23] The abundance of H^+ in acids is detrimental to the thermodynamic processes of the OER compared to basic media, resulting in the acidic OER possessing a higher reaction energy barrier. The high energy barrier and the inherent slow kinetics hinder efficient water decomposition for hydrogen production. Therefore, efficient and stable catalysts that can efficiently accelerate the reaction kinetics and reduce the reaction energy barrier are needed.[24–27]

To date, many novel high-performing electrochemical catalysts have been explored, such as carbon-based materials, transition metal oxides, transition metal oxygen hydroxides and their composites.[28] Typically, OER processes involve the conversion of transition metal-based catalysts to oxides at high electrical potentials, leading to valence transitions and

structural disruption. Among the many transition metal-based catalysts, manganese oxides (MnO_x) have an abundance of valence states and crystal structures that exhibit excellent electrocatalytic performance in various electrochemical reactions, with MnO_2 showing unique catalytic activity and stability for the acidic OER, making MnO_2-based materials show unprecedented promise in the field of OER. Among them, MnO_2-based materials have shown unprecedented prospects in the field of OER. Although manganese-based oxides do not have the same electrocatalytic activity as other metals, such as nickel, cobalt and iron, manganese is the only metal involved in the natural photosynthetic cycle, ensuring its sustainability and renewability.[29–32] MnO_2 has many advantages that have a positive effect on the OER, such as (1) the presence of a large number of defect edges that can improve the catalytic activity by providing more load sites of noble metals; (2) MnO_2 has various morphologies and electronic structures that are tunable and can meet different applications; and (3) the strong corrosion resistivity in acidic environments. The diversity of MnO_2 is due to the different stacking and connection modes of its $[MnO_6]$.[33] α-MnO_2 has an orthogonal unit cell, whose lattice is composed of a $[2 \times 2][1 \times 1]$ tunnel structure, and the tunnel size is approximately 4.6 Å. β-MnO_2 has a rutile structure, whose lattice is composed of a $[1 \times 1]$ tunnel structure, and the tunnel size is approximately 2.3 Å. The lattice of γ-MnO_2 is composed of a $[1 \times 1][2 \times 2]$ tunnel structure, and the tunnel size is approximately 0.7 Å.[34–36] Because MnO_2 has many factors such as low-cost property, abundant defect edges, regular tunneling structure, and unique acid resistance which provides assurance of the catalytic stability of the acidic OER, MnO_2-based materials have a good prospect in the field of OER. The OER process induced by MnO_2 involves the reversible cycle among the oxidation states of Mn^{2+}, Mn^{3+} and Mn^{4+} and the surface adsorption and desorption of oxygen species.[37–40] Generally, Mn^{3+} occupied by a single electron in the *e.g.* orbital

Jing Li is an Associate Researcher and Doctoral Supervisor at the College of Chemical Engineering and Technology, Hainan University. She received her Doctor of Engineering degree from South China University of Technology in 2019. In 2020, she joined the College of Chemical Engineering and Technology, Hainan University, and joined the innovation team of "Marine Clean Energy" in the National Key Laboratory of Marine Resources Utilization in the South China Sea. Her research interest covers the design and controlled synthesis of nano-catalytic materials for water/seawater electrolysis.

Xinlong Tian is Professor and Doctoral Supervisor of MRU; he received his doctorate in engineering from South China University of Technology in 2016, which was followed by his postdoctoral research at Huazhong University of Science and Technology. In March 2019, he joined MRU as the leader of the "Clean Energy in the Ocean" innovation team. He has long been engaged in the design of functionalized nanocatalytic materials and their basic applied research in the field of environment and energy, including electrocatalysis, hydrogen production by photo/electrolysis of seawater, hydrogen fuel cells and combustible ice conversion.
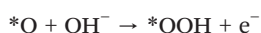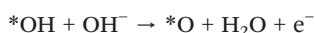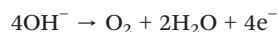
is considered to be conducive to the OER process. The high spintronic configuration of Mn^{3+} constitutes a highly active site for oxygen evolution. As the active species of the manganese dioxide catalyst, Mn^{3+} increases the adsorption capacity of OH^-, as well as shortens the adsorption and desorption time of reaction intermediates on the surface, and usually the increase of Mn^{3+} means more oxygen vacancies. Because of the Jahn–Teller activity, Mn^{3+} is the most unstable oxidation state of Mn, so stabilizing Mn^{3+} is essential to improve the electrocatalytic performance of MnO_2.[41–43]

In recent years, several studies have developed MnO_2-based OER catalysts that showed superior catalytic activity in acidic environments, which is very promising for applications in water electrolysis devices. To summarize the latest research progress in this field, this review focuses on the application of MnO_2-based catalysts in the OER. First, the OER mechanisms based on MnO_2 materials were summarized, including the traditional adsorbent evolution mechanism (AEM) and the emerging lattice-oxygen-mediated mechanism (LOM). Then, the development status and prospects of MnO_2-based OER catalysts are discussed. Finally, summarizing the difficulties in the research of MnO_2-based catalysts at present, some perspectives are proposed, which are expected to be helpful in the field of MnO_2-based OER catalyst development.
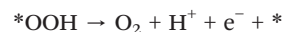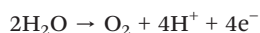
2 Mechanism and basic principle of the oxygen evolution reaction

The OER involves a four-electron transfer reaction in the process of water electrolysis. The OER has a higher reaction barrier and inherently slower kinetics than the HER, which makes the OER more difficult to occur and hinders effective hydrogen production from the electrolytic water. Electrolysis of water can be carried out in a wide range of pH values, including acidic, neutral and alkaline media.

In the alkaline and neutral media, the OER is usually considered to proceed in the following four steps:

$$4OH^- \rightarrow O_2 + 2H_2O + 4e^-$$

$$* + OH^- \rightarrow *OH + e^-$$

$$*OH + OH^- \rightarrow *O + H_2O + e^-$$

$$*O + OH^- \rightarrow *OOH + e^-$$

$$*OOH + OH^- \rightarrow O_2 + H_2O + e^- + *$$

In an acidic medium, the OER proceeds in the following four steps:

$$2H_2O \rightarrow O_2 + 4H^+ + 4e^-$$

$$* + 2H_2O \rightarrow *OH + H_2O + H^+ + e^-$$

$$*OH + H_2O \rightarrow *O + H_2O + H^+ + e^-$$

$$*O + H_2O \rightarrow *OOH + H^+ + e^-$$

$$*OOH \rightarrow O_2 + H^+ + e^- + *$$

where * represents the active site of the OER. In the acidic medium, two water molecules are adsorbed onto the catalytic site and undergo three subsequent steps of protonation to form *OOH intermediates. Finally, *OOH is oxidized by the electron transfer process, which releases O_2 and restores the active site of the initial reaction. In contrast, in alkaline and neutral media, OH^- adsorbs onto the reactive site to form *OH and then undergoes proton coupling and electron depletion to form *O species. *O reacts with OH^- to form *OOH. *OOH eventually binds to another OH^- to release O_2. Although the OER mechanisms seem different in acidic and alkaline electrolysis, both acidic and alkaline electrolysis involve four basic steps and the same oxygen-adsorbing intermediates (*OH, *O, and *OOH).[44–46]

Compared with the other two media, the abundant H^+ ions in acid are intermediate products of the OER, which hinder the reaction process of the OER thermodynamically and increase the reaction energy barrier. The catalytic activity is determined by the free energy difference of each basic step (ΔG). It is well known that the step with the highest Gibbs free energy is the rate determining step (RDS).[47,48] For MnO_2, the free energy spectrum shows that the RDS is the formation of *O, corresponding to $\Delta G = 1.95$ eV, and the corresponding overvoltage is 0.72 V (Fig. 1). The OER involves a variety of reaction intermediates, and the binding energy of each intermediate cannot be independently regulated. Therefore, a high overpotential is still required to drive the reaction. The theoretical limit for calculation is approximately 370 ± 100 mV.[49–51] However, many of the reported catalysts have broken through the theoretical overpotential limit of the traditional AEM, which proves that there are other oxygen evolution mechanisms in addition to the traditional AEM. At present, the LOM has been regarded as one of the possible mechanisms to explain the low overpotential for the
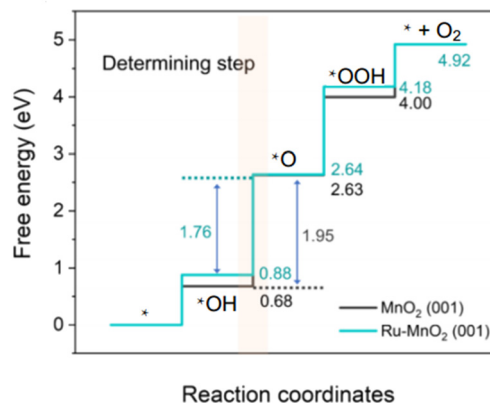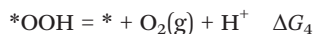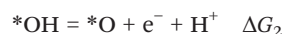

Fig. 1 Calculated Gibbs free-energy diagram of the OER for MnO_2 and $Ru–MnO_2$. Reprinted with permission from ref. 9. Copyright 2022, *Nano Res.*

OER.[52–54] The essential difference between the two mechanisms is that the LOM, including active lattice oxygen participating in the OER, reduces the reaction overpotential and improves the activity of the catalyst.[55–57] However, the oxygen vacancy defect caused the active species to detach from the surface of the catalyst, resulting in the rapid degradation of the electrocatalysts.[58–60] Therefore, balancing the activity and stability of the electrocatalysts, we should regulate the participation of active lattice oxygen in the OER. The reaction mechanisms of both the AEM and LOM, as well as some strategies for controlling active lattice oxygen participation in the OER, are reviewed in detail below, which may inspire the study of optimizing OER catalysts.

2.1 Adsorbate evolution mechanism (AEM)

The AEM is generally considered to involve four cooperative proton–electron transfer reactions centered on active metal sites. As shown in the equations

$$* + H_2O = *OH + e^- + H^+ \quad \Delta G_1$$

$$*OH = *O + e^- + H^+ \quad \Delta G_2$$

$$* + H_2O = *OOH + e^- + H^+ \quad \Delta G_3$$

$$*OOH = * + O_2(g) + H^+ \quad \Delta G_4$$

Water molecules are adsorbed onto the reactive sites through an electrooxidation process, forming *OH adsorbed at the M site (*), which then undergoes proton coupling and electron removal to form *O species, and the O–O bond formation step allows *O to react with another water molecule to form *OOH. Finally, *OOH is oxidized by an electron transfer process to release O_2 and restore the initial M-site. According to the AEM, the OER involves multiple oxygen reaction intermediates such as *OH, *O and *OOH, as displayed in Fig. 2. The binding energies of the intermediates are linearly correlated and follow the scaling relationship $\Delta G_{OOH} = \Delta G_{OH} + 3.2 \pm 0.2$ eV.[61,62]

The OER overpotential can be described by the following equation:

$$\eta = \max[\Delta G_2, \Delta G_3]/e - 1.23 \text{ V}$$
$$= \max[(\Delta G*O - \Delta G*OH), (\Delta G*OOH - \Delta G*O)]/e - 1.23$$
$$= \max[(\Delta G*O - \Delta G*OH), 3.2 \text{ eV} - (\Delta G*O - \Delta G*OH)]/e - 1.23$$

The value of $\Delta G*O - \Delta G*OH$ is a unique descriptor for OER activity. Plotting η as a function of $\Delta G*O - \Delta G*OH$ yields Fig. 3, a universal volcanic relationship independent of the catalyst.[49,63,64]

Based on the reaction principle of the AEM, it is reasonable to propose strategies for optimizing OER catalysts:

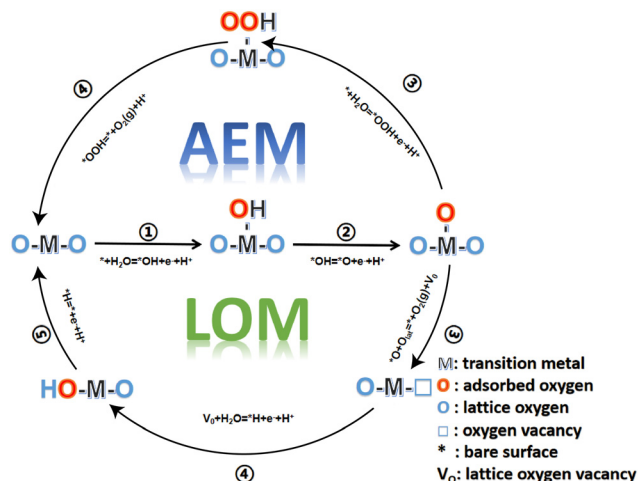(1) Adjust the binding strength of reaction intermediates on the surface.

Fig. 2 Adsorbate evolving mechanism (AEM) and lattice oxygen mechanism (LOM).

(2) The linear proportional relationship is broken stabilizing *OOH without affecting the adsorption of *OH.

(3) Good redox reaction center.

2.2 Lattice-oxygen-mediated mechanism (LOM)

The AEM is limited by the linear scaling relationship and involves a variety of oxygen reaction intermediates. The theoretical overpotential limit is 370 mV ± 100 mV. However, many studies have shown that the theoretical limit has been broken, which proves that there are other OER reaction mechanisms in addition to the AEM. The concept of the LOM where lattice oxygen participates in the reaction was first proposed by Damjanovic and Jovanovic in 1976.[45] Later, in 2015, Binninger and his co-workers put forward more formal descriptions and coined the term lattice oxygen evolution reaction.[49,56] The proposed LOM does not exclude the possibility that the binding energy of intermediates is
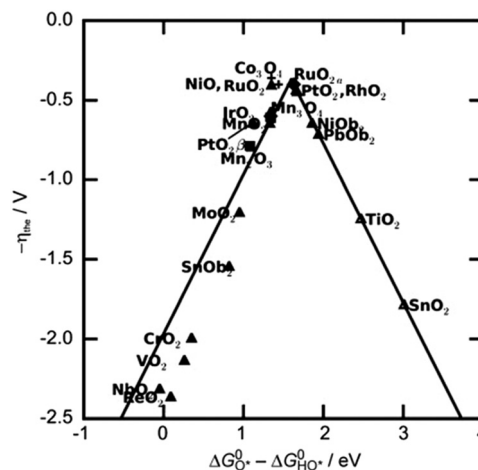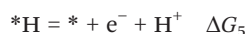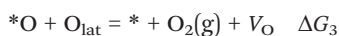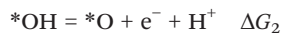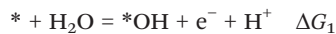

Fig. 3 OER volcano map of transition metal-based oxides. Reprinted with permission from ref. 49. Copyright 2021, *Small*.

still a valid activity descriptor. This clearly indicates that the dynamic catalyst surface needs to be considered, where the active site is not limited to the metal center (Fig. 4).

The LOM includes active lattice oxygen to participate in the OER and promote O–O coupling. As shown in the equations:

$$* + H_2O = *OH + e^- + H^+ \quad \Delta G_1$$

$$*OH = *O + e^- + H^+ \quad \Delta G_2$$

$$*O + O_{lat} = * + O_2(g) + V_O \quad \Delta G_3$$

$$V_O + H_2O = *H + e^- + H^+ \quad \Delta G_4$$

$$*H = * + e^- + H^+ \quad \Delta G_5$$

In a typical LOM, the first two steps are the same as those in the AEM by forming *O. Then, the formed *O couples with the lattice oxygen to release oxygen molecules, and oxygen vacancies are formed in the lattice at the same time. Finally, the vacancy can be refilled by the migration of OH⁻ from solution.

The LOM can bypass the generation of intermediate OOH*, thus avoiding the scaling relation between the adsorption energy of OH* and OOH*.[65] In this mechanism, lattice oxygen participates in the water oxidation process.[60,66] Therefore, to trigger the LOM, the O_{2p} band needs to be upshifted to closely approximate the Fermi level (EF), thereby increasing its orbital overlap with the metal d band (M–O bond covalency) and making the redox of lattice oxygen more energetically favorable.[67,68]

Although avoiding the scaling relationship between the adsorption energy of OH* and OOH* can reduce the OER overpotential, a large number of studies have shown that the enhanced OER kinetics are often offset by structural instability, which is mainly due to the cationic dissolution of M under anodic acid conditions.[69,70] Worse yet, the dynamic formation of a large number of oxygen vacancies (V_O) in the

OER process drives the bulk lattice oxygen to migrate to the surface to supplement the surface V_O, resulting in bulk phase remodeling and insufficient persistence. Therefore, although LOM-based catalysts have higher catalytic efficiency, they are considered uncompetitive in terms of stability and feasibility in practical applications.[71,72] Currently, there are two main solutions for resolving the stability issue: (1) choosing acid-stable reactive sites to combat lattice oxygen vacancies by slowing cation dissolution. (2) Adjusting the coordination environment to prevent lattice oxygen migration and excessive oxygen vacancies.

Therefore, several materials have been developed to achieve this goal. Among them, MnO_x shows excellent electrocatalytic performance in various electrochemical reactions, which not only has low cost and high abundance but also has rich valence and crystal structure. More importantly, MnO_2 based materials have catalytic activity and stability in the acidic OER and have been regarded as promising candidates for water electrolysis, and their recent progress will be discussed below.

3 Manganese dioxide based catalysts for an efficient OER

Recent studies have shown that the Mn^{3+} species with an antibonding electron configuration is the active phase of the OER in MnO_2-based catalysts.[49,73] The OER activity of any transition metal-based catalyst is generally highly dependent on the oxidation state of the corresponding metal. Monoelectron-occupied Mn^{3+} in the e.g. orbits are regarded to favor the hydrooxidation kinetics-electrolyte interface at the electrodes.[74] Monoelectronic occupancy in the e.g. orbital results in strong Jahn–Teller distortion, leading to the conversion of Mn–O to O–O, which provides a superior adsorption active site for oxygen-containing intermediates.[75] However, the OER process involves the reversible cycle between the oxidized states of Mn^{2+}, Mn^{3+}, and Mn^{4+}, as well as the surface adsorption and desorption of oxygen species. Since Mn^{3+} is the most unstable oxidized state of Mn, stabilizing Mn^{3+} is essential to improve the electrocatalytic stability of MnO_2.[76,77] In this section, the research progress of MnO_2-based OER catalysts in recent years is reviewed. Reasonable design and prospective research directions are also presented.

3.1 Single MnO_2 catalysts

The electrocatalytic activity of MnO_2 is strongly controlled by its morphology and crystal structure. By using different synthesis methods, different phases of manganese oxide with different properties can be formed, including one-dimensional tunnel type, two-dimensional layered compound and three-dimensional spinel structure.[54,74] Table 1 summarizes all crystal symmetries, lattice parameters and characteristics of different phases of some manganese dioxide. In addition, MnO_2 nanomaterials have the
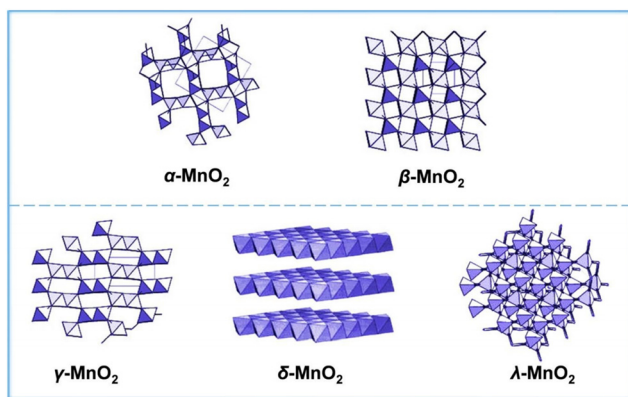

Fig. 4 Crystal structures of α-MnO₂, β-MnO₂, γ-MnO₂, δ-MnO₂, and λ-MnO₂. Reprinted with permission from ref. 110. Copyright 2018, Elsevier.

characteristics of morphological complexity (sea urchin like structure, flower, tube, plate, ball, wire, etc.). MnO_2 nanomaterials with different configurations have different sizes and electrocatalytic properties.

3.1.1 Effect of crystal form on catalytic performance. As shown in Fig. 2, the diversity of crystals is mainly due to the different stacking and connection modes of $[MnO_6]$ units in MnO_2.[78,110] The crystal structures of α-MnO_2, β-MnO_2 and γ-MnO_2 show 1D tunnels, λ-MnO_2 shows a 3D spinel structure, and δ-MnO_2 has 2D layered compounds.[40] The basic structural unit of α-MnO_2 is composed of a $[MnO_6]$ octahedron double chain, and α-MnO_2 is present as (1×1) and (2×2) tunnels.[79] The tunnel structure of MnO_6 with sizes of 1.89 Å and 4.6 Å constitutes an octahedron tunnel of α-MnO_2, which easily stabilizes ions and water molecules, and the oxygen vacancy generated in the structure of α-MnO_2 is a method to improve the catalytic activity.[80] Compared with other crystal forms, α-MnO_2 has better catalytic potential due to its high activity specific surface area, large aspect ratio, high active site density, low charge transfer resistance and high electron conductivity. The structure of β-MnO_2 is composed of $[MnO_6]$ octahedron single chains, which are joined by vertex sharing and form a (1×1) tunnel structure.[81] The narrow tunnel structure (1.89) makes it difficult for ions to diffuse into the bulk after undergoing electrochemical intercalation, which results in the poor electrochemical activity of traditional β-MnO_2. Defects in γ-MnO_2 crystals are considered favorable catalytic sites for the OER, so γ-MnO_2 has good prospects for the OER.[82] The interlayer space of the δ-MnO_2 structure is occupied by heterogeneous atoms to stabilize the layer structure. There are two typical structures: triangular and hexagonal. The unique layer structure of δ-MnO_2 enables it to have a larger tunnel specific surface area, abundant defects and adjustable resistivity.[78] λ-MnO_2 has a typical spinel structure. This material is more conducive to the implantation and removal of external ions than other crystallized manganese dioxide. In addition to the above five crystal forms, MnO_2 has many other crystal forms, but most of them are not suitable for OER catalysts. Compared with other crystal forms, α-MnO_2 and γ-MnO_2 are more suitable as carriers for the OER catalyst. The large tunnel structure of α-MnO_2 can accommodate some of the discharge products, making it a potentially effective catalyst. γ-MnO_2 induces abundant defects that are favorable catalytic sites for the OER. In general, α-MnO_2 and γ-MnO_2 with a large tunnel structure and abundant defects are more suitable as carriers of the OER catalyst.

3.1.2 Manganese dioxide catalysts with different morphologies. The electrocatalytic performance of the same type of MnO_2 is also different, mainly because the morphology is also important to the electrocatalytic performance. This section reviews the recent progress in the optimization of MnO_2 electrocatalytic performance by morphology engineering. Nakamura et al.[83] synthesized β-MnO_2 bipyramids and β-MnO_2 nanowires. The correlation between the stability of the intermediate and the crystal plane was confirmed for the first time by monitoring the electrochemical OER surface intermediates on rutile MnO_2 with different crystal plane orientations. The performance of the catalyst was improved by optimizing the surface electronic state and adjusting the reaction intermediates. It provides a possibility of surface engineering technology. Li et al.[84] first explained the atomic-level mechanism of the solid-phase transition of spinel-layer Mn_3O_4 in water electrolytes. At high voltage (>1 V), $H_{0.5}MnO_2$ is the transition precursor, which is transformed into a δ-MnO_2 layer by solid–solid phase deformation, accompanied by dissolution of Mn, dislocation, layer breakage and intercalation of water/cations. This results in the formation of various possible defect structures, and first-principles calculations show that the special edge locations with adjacent Mn vacancies provide the best OER activity, with an overpotential of 590 mV, which is 190 mV lower than that of the original MnO_2.

The research progress of α-MnO_2 with different morphologies is reviewed here. Table 3 summarizes the properties of α-MnO_2 with different morphologies. Yang et al.[85] reported that a polyionic liquid (IL)-assisted hydrothermal method regulates the crystal phase and nanostructure morphology of MnO_2 (Fig. 5a), enabling it to have great oxygen evolution activity. The overpotential at 10 mA cm^{-2} is 394 mV (Fig. 5b), and the Tafel slope is 49 mV dec^{-1}. It also demonstrated that the surface immobilized IL promotes the formation and stabilization of oxygen vacancies on the surface of α-MnO_2 nanowires. Zhou et al.[59] reported a one-step hydrothermal synthesis of typical MnO_2 electrocatalysts with optimized structure and electrochemical properties. The conversion of δ-MnO_2 to α-MnO_2 can be induced by simply adjusting the hydrothermal time. Nanowires grown in situ on nickel foam have a large surface area, easy access to active sites and good charge transfer efficiency. The prepared α-MnO_2 nanowires (Fig. 5c) exhibit excellent catalytic performance for the OER in Fig. 5d (OER overpotential is 450 mV at 50 mA cm^{-2}). Chen et al.[86] synthesized an unusual α-MnO_2 nanowire network (NWN)

Table 1 Summary of common MnO_2 crystal forms

Compound	Mineral	Crystal symmetry	Lattice parameters (Å)	Features
α-MnO_2	Hollandite	Tetragonal ($I4/m$)	$a = 9.96$; $c = 2.85$	(2×2) tunnel
β-MnO_2	Pyrolusite	Tetragonal ($P42/mnm$)	$a = 4.39$; $c = 2.87$	(1×1) tunnel
γ-MnO_2	Nsutite	Complex tunnel (hex.)	$a = 9.65$; $c = 4.43$	$(1 \times 1)/(1 \times 2)$
δ-MnO_2	Birnessite	Rhombohedral ($R\bar{3}m$)	$a_{hex} = 2.94$; $c_{hec} = 21.86$	$(1 \times \infty)$ layer
λ-MnO_2	Spinel	Cubic ($Fd3m$)	$a = 8.04$	(1×1) tunnel

© 2023 The Author(s). Co-published by the Institute of Process Engineering, Chinese Academy of Sciences and the Royal Society of Chemistry

Ind. Chem. Mater., 2023, **1**, 312–331 | **317**

Table 2 Summary of the different morphologies of α-MnO$_2$

Catalyst nanostructure	Electrolyte	Method	BET surface area	OER/η (mV)@j (mA cm^{-2})
α-MnO$_2$ nanoflower	0.1 M KOH	Hydrothermal	52.4	890@5
α-MnO$_2$ nanowires	0.1 M KOH	Hydrothermal	24.25	527@10
α-MnO$_2$ nanowire network	0.1 M KOH	Hydrothermal	15.8	467@10
α-MnO$_2$ microspheres	0.1 M KOH	Hydrothermal	22.80	570@5
α-MnO$_2$ nanowires (IL)	0.1 M KOH	Hydrothermal	—	394@10
α-MnO$_2$ nanowires (foam nickel)	0.1 M KOH	Hydrothermal	—	450@10

**Table 3** Summary of recent MnO$_2$ based catalysts

Catalysts	Method	Electrolyte	OER/η (mV)@j (mA cm^{-2})	Tafel slope (mV dec^{-1})	Stability
12Ru/MnO$_2$	Stirred at room temperature (single-atom doped)	0.1 M HClO$_4$	161@10	29.4	200 h at 10 mA cm^{-2}
Ir–MnO$_2$	Thermal decomposition (single-atom doped)	0.5 M H$_2$SO$_4$	218@10	59.61	650 h at 10 mA cm^{-2}
Ru–MnO$_2$	Electrodeposition (single-atom doped)	1.0 M KOH	240@10	48	100 h at 30 and 100 mA cm^{-2}
Au–MnO$_2$	Hydrothermal	0.1 m KOH	320@10	68	—
MPNF–MnO$_2$	Pulse electrodeposition	1.0 M KOH	363.5@10	94.7	24 h at 10 mA cm^{-2}
Co$_3$O$_4$–MnO$_2$	Chemical vapor deposition	In alkaline seawater pH = 13.5	450@10	40	—
Ti/TiO$_2$-NTs/PbO$_2$–CNTs–MnO$_2$	Electrodeposition	1.53 M H$_2$SO$_4$	410@50	—	30 h at 50 mA cm^{-2}
MnO$_2$/BCS	Hydrothermal	1.0 M KOH	170@10	31.43	48 h at 1.45 V
MnO$_2$@MOF-5	Stirred at room temperature	1.0 M NaOH	324@10	71	6000 s at 10 mA cm^{-2}
nwMnO$_2$–nsNi(OH)$_2$	Hydrothermal	1.0 M KOH	410@10	68	300 h at 10 mA cm^{-2}
0.25% B–MnO$_2$	Grind	0.066 M H$_3$PO$_4$	425@1	95	12 h at 1 mA cm^{-2}
Fe–MnO$_2$/NF	Stirred at room temperature	1.0 M KOH	330@20	51	24 h at 20 mA cm^{-2}
FeC/MnO$_2$	Carbonization	1.0 M KOH	250@10	39.81	40 h at 10 mA cm^{-2}
MnO$_2$/(Fe,Ni)$_3$S$_4$	Hydrothermal	1.0 M KOH	220@10 325@500	44.70	20 h at 10/100 mA cm^{-2}
VO-MnO$_2$–NF	Electrodeposition	1.0 M KOH	300@10	84	40 000 S at 10 mA cm^{-2}
Ni–MnO$_2$	Hydrothermal	0.1 M KOH	445@10	86	10 h at 10 mA cm^{-2}
Co$_3$O$_4$/MnO$_2$–CNTs	Hydrothermal	6 M KOH	400@10	—	140 h at 20 mA cm^{-2}
Ni–Fe–K$_{0.23}$MnO$_2$ CNFs-300	Hydrothermal	1.0 M KOH	270@10 320@100	42.3	24 h at 10 mA cm^{-2}
DV-MnO$_2$	Li-EDA	1 M KOH	260@10	63	100 h at 10 mA cm^{-2}
CDs0.15–MnO$_2$	Microwave reaction	1 M KOH	343@10	43.6	36 h at 10 mA cm^{-2}
NF–Ni$_3$S$_2$/MnO$_2$	Hydrothermal	1.0 M KOH	260@10	61	48 h at 100 mA cm^{-2}
NiCe/MnO$_2$	Oil bath	1.0 M KOH	170@10	42	70 h at 10 mA cm^{-2}
Co–MnO$_2$|OV	Hydrothermal	1.0 M KOH	279@10	75	12 h at 10 mA cm^{-2}

without any surfactants through a mild hydrothermal reaction. The α-MnO$_2$ NWN (Fig. 5e) exhibited excellent catalytic activity with an OER overpotential of 467 mV at 10 mA cm^{-2} (Fig. 5f). In a network, nanowires are connected to each other through nodes in all directions and the three-dimensional network structure is formed by nodes connecting endlessly in a node-like manner. The unique network structure results in higher hydrophilicity and conductivity, both of which are positive factors for efficient electrocatalysts. MnO$_2$ nanomaterials with different configurations have different sizes and electrocatalytic properties. Table 2 summarizes the size and electrocatalytic properties of α-MnO$_2$.

Manganese dioxide of the same crystal form has a larger specific surface area and better conductivity, and has better OER catalytic properties. Macroscopically, the strategies for optimizing the activity of MnO$_2$ electrocatalysts mainly include improving the intrinsic surface activity, improving the mass diffusion efficiency, enhancing the charge transfer capability, etc. These strategies point out the way for optimizing the performance of MnO$_2$ electrocatalysts: increasing the specific surface area, increasing the porosity, improving the conductivity, etc. Fortunately, research on optimizing the activity of MnO$_2$ electrocatalysts through morphology engineering has made great progress. MnO$_2$ nanomaterials have morphological complexity (sea urchin like structure, flower, tube, plate, ball, wire, etc.). At present, research on the morphology of MnO$_2$ tends to be more microscopic, such as increasing defect edges, tunnel fixed ions, phase conversion, and a series of microscopic optimization methods. Based on the optimization of morphology engineering, the activity of the MnO$_2$
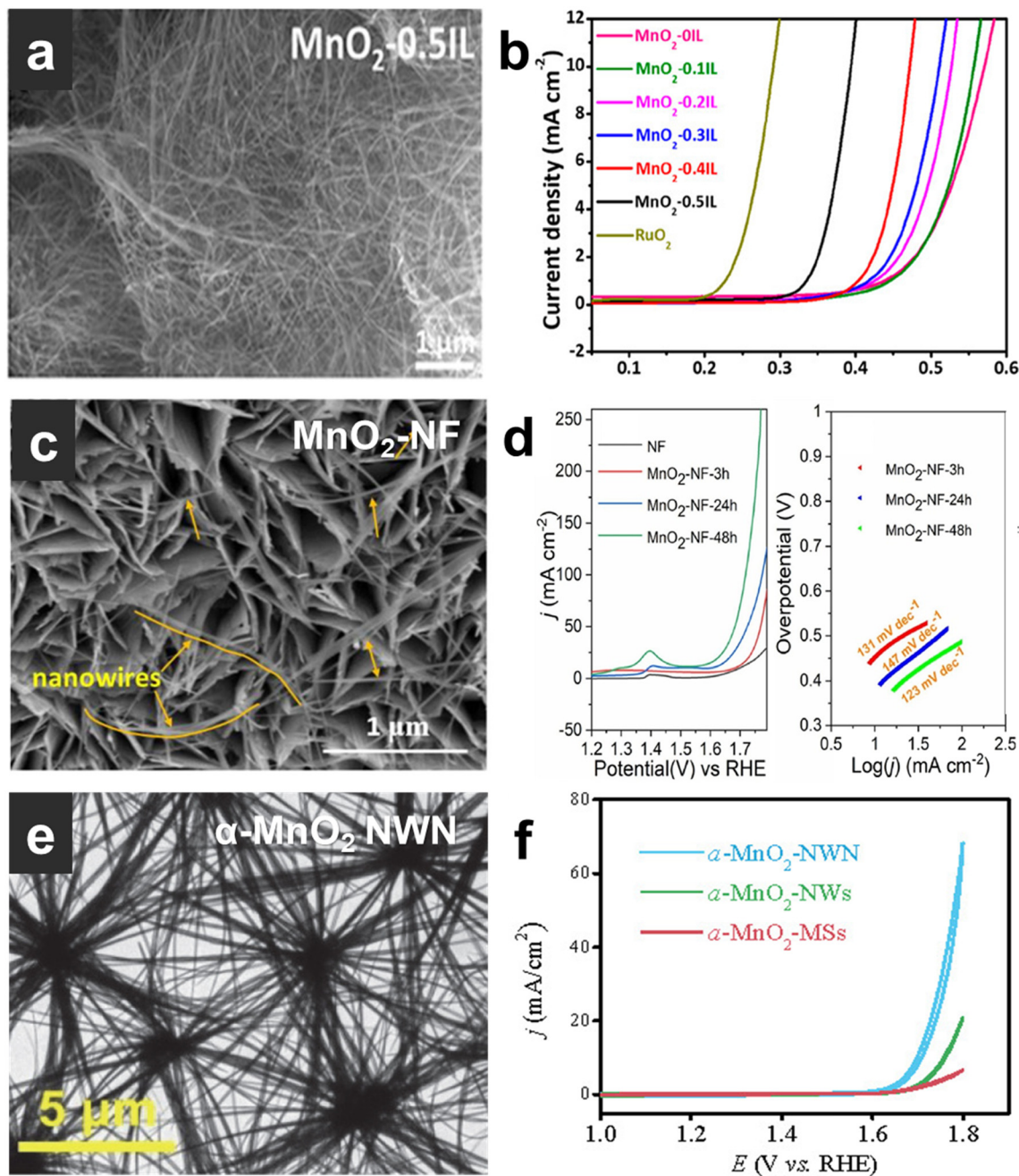
Fig. 5 (a) (c) and (e) TEM images of MnO$_2$-0.5IL, MnO$_2$–NF, and α-MnO$_2$ NWN. (b) (d) and (f) Electrocatalytic OER performance of MnO$_2$-0.5IL, MnO$_2$–NF, and α-MnO$_2$ NWN. Reprinted with permission from ref. 85. Copyright 2018, ACS Catal. Reprinted with permission from ref. 59. Copyright 2022, *Chem. Eng. J.* Reprinted with permission from ref. 86. Copyright 2021, *Chin. J. Catal.*

electrocatalyst was further optimized. The main problem is the stability of Mn^{3+}, which is a very promising research direction.

3.2 MnO$_2$-based composite catalysts

Although the electrocatalytic activity of single MnO$_2$ is not as high as that of other metal oxides, MnO$_2$ has a large number of unsaturated edges, various crystal structures and electronic structures, and rich oxidation states, which make it a great

OER catalyst carrier. Coupling MnO$_2$ with precious metal and/or non-precious metal-based elements has been proven to be a promising strategy to enhance the OER performance. This section mainly reviews the recent progress of MnO$_2$-based catalysts, and Table 3 summarizes the recent loading mode and electrocatalytic performance of MnO$_2$-based catalysts.

3.2.1 Precious-metal catalyst supported on manganese dioxide. The introduction of ultra-low content and high-activity noble metal elements into transition metal-based

© 2023 The Author(s). Co-published by the Institute of Process Engineering, Chinese Academy of Sciences and the Royal Society of Chemistry

Ind. Chem. Mater., 2023, **1**, 312–331 | **319**

catalysts is an effective way to construct high-performance catalysts, in which doped noble metal elements act as OER active sites to increase catalytic activity. The doping modes of noble metal elements are mainly divided into nanocluster doping and single-atom doping. The difference between the two doping modes mainly lies in the existing forms of doping elements. A large number of studies have been devoted to the synthesis of stable OER catalysts by combining highly active noble metal elements with transition metal oxides to improve the utilization efficiency and catalytic performance of noble metal materials.

Qin et al.[87] investigated the topological effects on the OER activity in which they carefully investigated partially Ru-substituted β-MnO_2, α-MnO_2, and τ-MnO_2 to illustrate the structure–property performance correlation. At 1.53 V, the best catalyst β-MnO_2–Ru achieved a high TOF of 2022.2 h^{-1} that is 19.6-fold higher than that of the commercial RuO_2 benchmark. Moreover, it has been shown that Ru integration is not simply attaching to relatively inert metal oxides, but also adjusting the crystal structure of manganese dioxide to retroactively regulate the catalyst activity. Ghadge et al.[88] synthesized $(Mn_{0.8}Ir_{0.2})O_2$: 10F by loading Ir on α-MnO_2. The overpotential under 10 mA cm^{-2} is only 220 mV, and the stability exceeds 24 h. The reported results further demonstrate that if manganese dioxide can exhibit high conductivity and the desired electrochemical stability in acidic media, doping with some non-inert materials can alter the electronic structure and make it a potential anode catalyst for PEMWE.

Lee et al.[89] reported a Ru atomic array patch electrocatalyst supported on α-MnO_2 (12Ru/MnO_2) for the oxygen evolution reaction using *O and *OH as intermediates only. The oxidation pathway mechanism of heterogeneous catalysts (Fig. 6a) allows direct O–O radical coupling without producing oxygen vacancy defects and additional reaction intermediates (*OOH). 12Ru/MnO_2 has high activity and excellent stability, with an overpotential of 161 mV at 10 mA cm^{-2} (Fig. 6b), a Tafel slope of only 29.4 V dec^{-1} (Fig. 6c), and little degradation after 200 hours at 10 mA cm^{-2} (Fig. 6d). A large number of measurements, translocation characterizations and theoretical calculations of the OER on 12Ru/MnO_2 indicate that the OER is carried out through the oxidative pathway mechanism (OPM), and the key step is direct O–O base coupling. This unique reaction pathway enables Ru/MnO_2 to overcome the overpotential limitation imposed by the traditional AEM. The stability decay of 12Ru/MnO_2 is due to a combination of morphological and electronic characteristics. The dynamic cation exchange reaction between Ru and MnO_2 during the OER not only triggers the self-rebuilding of the electrocatalysts, but also ensures that leached Ru ions can be recaptured to support further reactions, thereby enhancing corrosion resistance. Ge et al.[90] synthesized Ir–MnO_2 by a single-atom Ir doping strategy with γ-MnO_2 (Fig. 6e). The mass activity of Ir–MnO_2 is more than 42 times that of commercial IrO_2. The overpotential under 10 mA cm^{-2} is only 218 mV (Fig. 6f), and the Tafel slope is only 59.61 V dec^{-1} (Fig. 6g). The stability of

Ir–MnO_2 exceeds 650 h (Fig. 6h), and the overpotential increases by only 15 mV. Moreover, due to the well-defined chelating environment of Ir, an increase in Ir–O covalence and its participation in lattice oxygen oxidation were observed. More importantly, the locally triggered LOM did not introduce structural evolution during the OER. The findings of this work may inspire the design of highly efficient acidic OER catalysts with low iridium content based on the local LOM to improve the intrinsic activity and stability. Liu et al.[91] developed an in situ electrochemical cation exchange method, and Ru/MnO_2 was prepared by filling cation vacancies in MnO_2 with Ru single-atoms (SAs). It has higher OER activity (240 mV at 10 mA cm^{-2}), which is 44 times higher than that of commercial RuO_2 catalysts, and has good stability (100 h at 30 and 100 mA cm^{-2}). The combination of Ru and MnO_2 creates an electron-rich environment at the Ru site. This strong local electric field effect enhances the electrolysis and dissociation as well as the OER activity. The strong local electric field effect is due to the strong synergistic coupling between Ru and metal materials, which can optimize the rate determining step (RDS) and inhibit the migration and aggregation of Ru atoms.

Among precious-metal catalysts supported by manganese dioxide, the oxides of Ru supported by manganese dioxide are complementary, because manganese dioxide itself has unique acid resistance but ordinary catalytic performance for the OER, while the oxides of Ru have high OER activity and low stability.[92] Therefore, the oxides of manganese dioxide and Ru can complement the activity and stability of the OER by regulating the oxygen evolution mechanism. Manganese dioxide supported Ir has strong combination strength. By combining the acidic OER stability of Ir and manganese dioxide, the catalytic stability of the OER can be further improved without sacrificing the performance of the OER by adjusting the lattice oxygen vacancy.

At present, more studies are biased toward single-atom doping into MnO_2 to improve the utilization of precious metals, obtain better catalytic performance, and reduce costs. The cluster is a transition state between single atoms and nanoparticles. Its geometric structure is very diverse, and it will transform into each other in two-dimensional to three-dimensional structure with different sizes.[93] The utilization rate of atoms is relatively low, and the dynamic structural change leads to the complicated study of the catalytic mechanism. A single atom doped catalyst is an ideal catalyst model for constructing a noble metal catalyst because of its high atom utilization efficiency.[94] When the dispersion of the loaded metal reaches the atomic level, its energy level structure and electronic structure will undergo fundamental changes. The highly uniform active sites and geometric configuration of single-atom doped catalysts are more conducive to the study of the catalytic mechanism. With regard to the mechanism of the OER, the current research is more inclined to focus on the LOM. The main problem is how to break the scale relationship between catalytic performance and stability, that is, how to improve the OER performance without affecting the stability of the catalyst. In
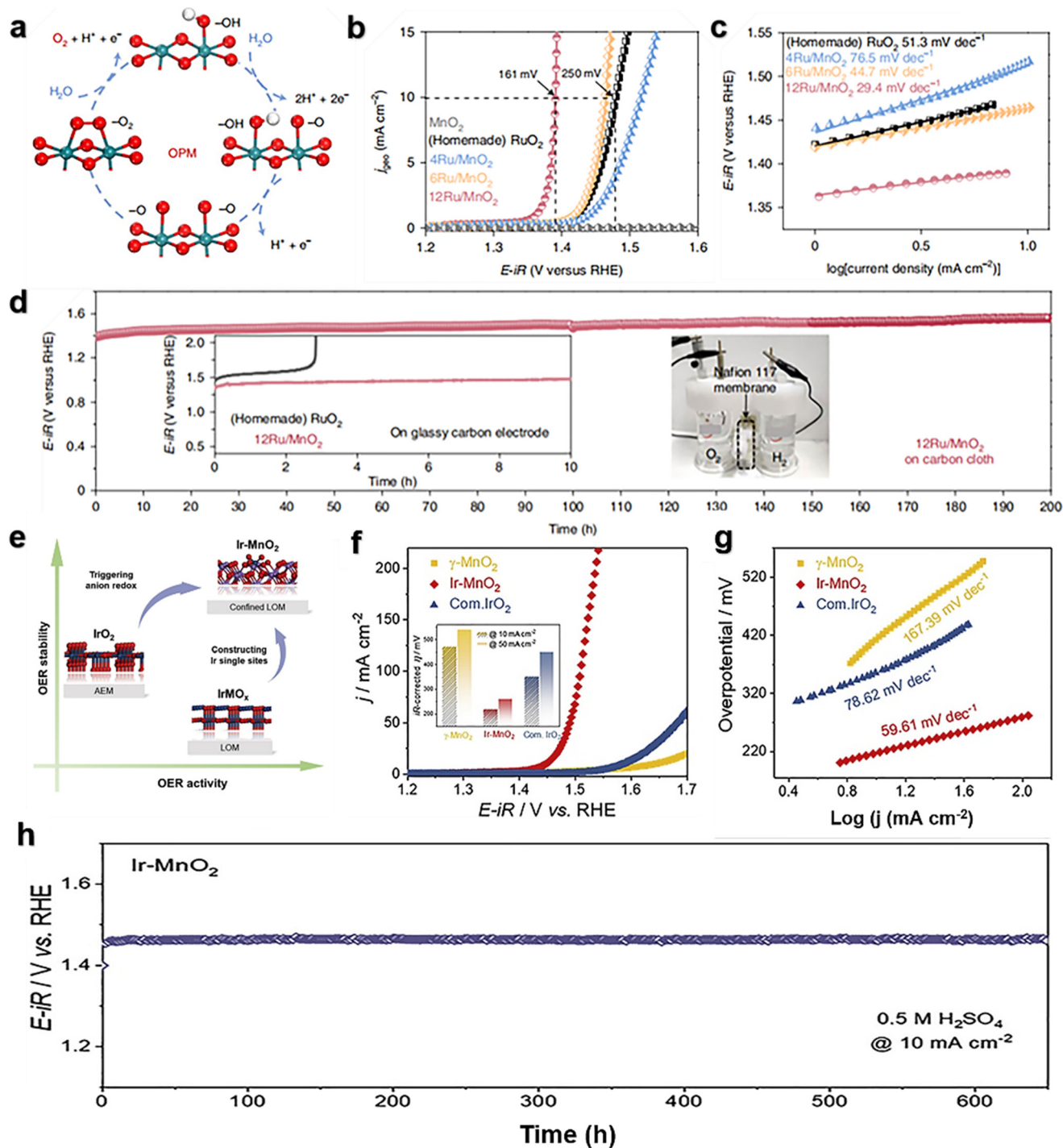
Fig. 6 (a) Oxide path mechanism (OPM); (b) electrocatalytic OER performance of MnO_2, Ru/MnO_2 and homemade RuO_2 in 0.1 M $HClO_4$; (c) Tafel slopes of MnO_2, Ru/MnO_2 and homemade RuO_2; (d) chronopotentiometric response of the $12Ru/MnO_2$ catalyst. Reprinted with permission from ref. 89. Copyright 2021, *Nat. Catal.* (e) The design of an Ir single-atom catalyst can trigger lattice oxygen oxidation locally while maintaining the stability of the bulk structure; (f) representative LSV curves of MnO_2, $Ir–MnO_2$, and commercial IrO_2 in 0.5 M H_2SO_4; (g) Tafel slope of MnO_2, $Ir–MnO_2$, and IrO_2; (h) chronopotentiometric response of $Ir–MnO_2$ for the OER at 10 mA cm^{-2}. Reprinted with permission from ref. 90. Copyright 2021, *Joule*.

addition to the AEM and LOM, recent studies have proposed an OPM for heterogeneous catalysts, which allows O–O radicals to be directly coupled without producing oxygen

vacancy defects and additional reaction intermediates (*e.g.*, *OOH), containing only *O and *OH as intermediates. More importantly, the active metal sites at appropriate locations

© 2023 The Author(s). Co-published by the Institute of Process Engineering, Chinese Academy of Sciences and the Royal Society of Chemistry

Ind. Chem. Mater., 2023, **1**, 312–331 | **321**

work together without the involvement of lattice oxygen under the OPM. Ideally, heterogeneous electrocatalysts based on the OPM can break the scale relationship without sacrificing stability, but the OPM has stricter requirements on the geometry of metal active sites than the AEM and LOM.[89,95] The fundamentals of the OPM are not yet well understood, and further study is still needed. How to control lattice oxygen vacancies is an urgent problem to be solved. A further question is whether single-atom-doped MnO_2-based catalysts are suitable for industrial water electrolysis. Single-atoms maintain excellent stability at low current densities. However, at high current densities, precious metal single-atoms are readily leached. Therefore, the problem of catalytic stability under the high current density of industrial electrolytic water still needs to be solved. At present, research on manganese dioxide loaded precious metals has made great progress, but there are still many problems that need to be solved.

3.2.2 Non-noble metal catalysts supported on manganese dioxide. Combining the undercoordinated sites on the surface of MnO_2 with a stable non-precious metal can inhibit the dissolution of MnO_2 and stabilize the catalytic sites.[96] In addition, the coupling of MnO_2 with transition metal-based elements can effectively regulate the electronic structure of MnO_2, optimize the free energy of adsorption/desorption of OER intermediates, and thus significantly enhance the intrinsic catalytic activity.[97] This section reviews the latest research on non-noble metal catalysts supported on manganese dioxide.

Yang et al.[98] fine-tuned the interlamellar environment of manganese dioxide nanoparticles by simple cation exchange with transition metal cations (Ni^{2+}, Co^{2+}, Cu^{2+}, Zn^{2+}, Fe^{3+}). The overpotential of 330 mV at a current density of 10 mA cm^{-2} is observed for the Ni-intercalated MnO_2 nanosheets. It is proved that Ni intercalation enhances Mn–O bonds perpendicular to the layer chain, which may promote the interlayer catalysis between Mn and thus promote the catalytic activity of the OER.

Many optimizations on Ni-doped manganese dioxide have been carried out in the latest studies. Zhang et al.[99] prepared co-doped MnO_2 ($NiCe/MnO_2$) nanosheets (NS) with oxygen vacancies (V_O) and abundant active sites using a defect strategy (Fig. 7a). In 1.0 M KOH, the overpotential is 170 mV@10 mA cm^{-2} (Fig. 7b), and the Tafel slope is 42 mV dec^{-1} (Fig. 7c). The $NiCe/MnO_2$ NS showed no significant decrease in activity and good stability after 70 h of cycling (Fig. 7d). On the one hand, the co-doping of Ce/Ni reduces the size of the catalyst and increases the specific surface area, which promotes the exposure of more active sites. On the other hand, heteroatom doping alters the species on the surface of the crystal, stimulates V_O formation, and thus activates the performance of the catalyst. Zhang et al.[100] developed a simple and controllable method (Fig. 7e) to prepare a self-standing tremella-shaped $MnO_2/(Fe, Ni)_3S_4$ hybrid catalyst, which significantly promotes the OER process in alkaline media. The optimum $MnO_2/(Fe, Ni)_3S_4$ electrodes require 220 and 325 mV to achieve current densities of 10 and 500 mA cm^{-2} (Fig. 7f), respectively. The Tafel slope is only 44.70 V dec^{-1} (Fig. 7g). In addition, the $MnO_2/(Fe,Ni)_3S_4$ electrodes exhibited excellent durability at 10 mA cm^{-2} and 100 mA cm^{-2} during the 20 h OER (Fig. 7h). It is also demonstrated that the long tremella structures composed of nanosheets are cross-linked, providing a considerable number of open pores. This porous three-dimensional structure increases the specific surface area of the catalysts and provides abundant OER active sites. At the same time, these nano-sized pores promote the transport of oxygen molecules and accelerate the OER. This pleated complex layer structure may facilitate charge transfer and rapid ion diffusion in the OER process. Xiong et al.[101] developed a thin Ni_3S_2/MnO_2 heterogeneous nanoarray ($NF–Ni_3S_2/MnO_2$) for overall water decomposition (Fig. 8a). The OER overpotential was 260 mV at 10 mA cm^{-2} (Fig. 8b) and was stable over 48 h at 100 mA cm^{-2} (Fig. 8c) in 1.0 M KOH. The construction strategy includes a simple two-step hydrothermal conversion, and the shape and composition of the hybrid nanoarray can be easily customized. The prepared $NF–Ni_3S_2/MnO_2$ with certain exposed interfaces and active sites integrates and optimizes the advantages of multilayered Ni_3S_2 and MnO_2, and achieves the expected fast kinetics and excellent performance of overall water decomposition in alkaline media. Liu et al.[102] reported a double-vacancy doped MnO_2 ultra-thin nanosheet ($DV-MnO_2$) (Fig. 8e). At a current density of 10 mA cm^{-2}, the OER overpotential was 260 mV (Fig. 8h), and the stability exceeded 100 h (Fig. 8j). The synergistic effect of anion-oxygen and cation-manganese vacancies (V_O and V_{Mn}) in manganese dioxide (MnO_2) nanotablets has been demonstrated to cause abnormal local lattice distortion and electronic modulation. These changes enrich the reachable active sites, increase the conductivity, enhance the hydrolytic dissociation steps, facilitate the intermediate adsorption–desorption, and thus promote the HER and OER kinetics. Synergistic DV (dual vacancies) can capture more active components through good adsorption, and faster electron transfer to these active components will promote the reaction kinetics. This proof-of-concept study provides a strategy for the rational design of excellent catalysts for water splitting and other related energy conversion reactions.

In manganese dioxide supported non-noble metal catalysts, in the first row of non-noble transition metals Fe, Co, Ni, Cu, and Zn, Ni intercalation enhances Mn–O bonds perpendicular to the layer chain, which may promote the interlayer catalysis between Mn and thus promote the catalytic activity of the OER. Later studies used further co-doping to optimize MnO_2-supported Ni catalysts.

Most studies on manganese dioxide doped with non-precious metal catalysts tend to be applied for the alkaline OER, which is mainly because the abundant H^+ in acid are not thermodynamically favorable for the OER.[42,103] Non-noble metal-based catalysts are easy to convert into oxides at high oxidation potentials, leading to valence transitions and structural damage. Based on the current research, the doping of non-precious metals has two basic roles:
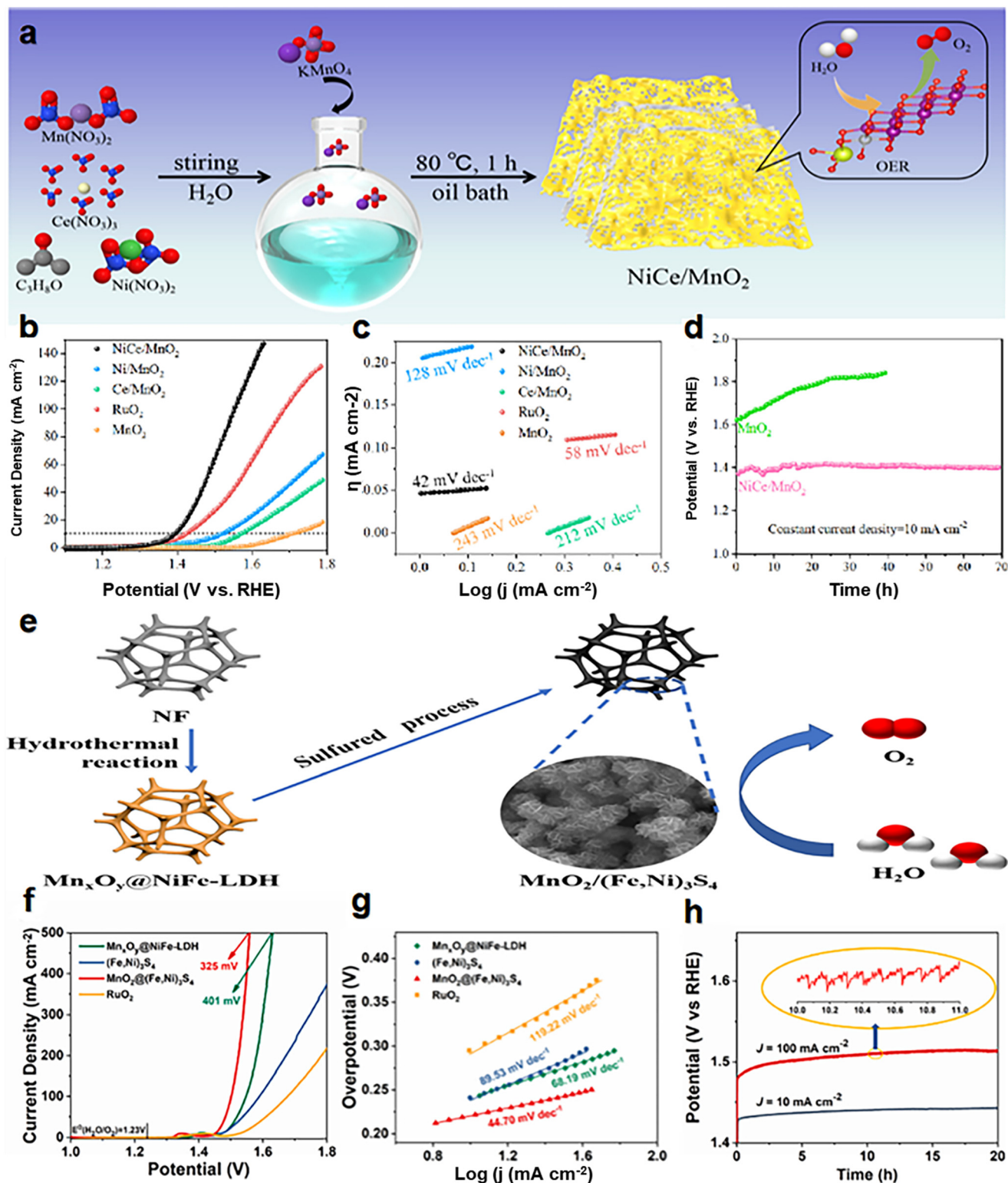
Fig. 7 (a) Schematic diagram of the NiCe/MnO₂ catalyst synthesis process; (b) electrocatalytic OER performance of NiCe/MnO₂; (c) Tafel slope of NiCe/MnO₂; (d) chronopotentiometric response of NiCe/MnO₂ and MnO₂. Reprinted with permission from ref. 99. Copyright 2022, ScienceDirect. (e) Schematic diagram of the MnO₂/(Fe,Ni)₃S₄ catalyst synthesis process; (f) electrocatalytic OER performance of MnO₂/(Fe,Ni)₃S₄; (g) Tafel slope of MnO₂/(Fe,Ni)₃S₄; (h) chronopotentiometric response of MnO₂/(Fe,Ni)₃S₄. Reprinted with permission from ref. 100. Copyright 2021 *J. Power Sources*.

(1) Controlling the morphology of MnO₂ is manifested by increasing the specific surface area, enhancing the conductivity and mass transfer rate, and exposing more active sites.

© 2023 The Author(s). Co-published by the Institute of Process Engineering, Chinese Academy of Sciences and the Royal Society of Chemistry

Ind. Chem. Mater., 2023, **1**, 312–331 | **323**
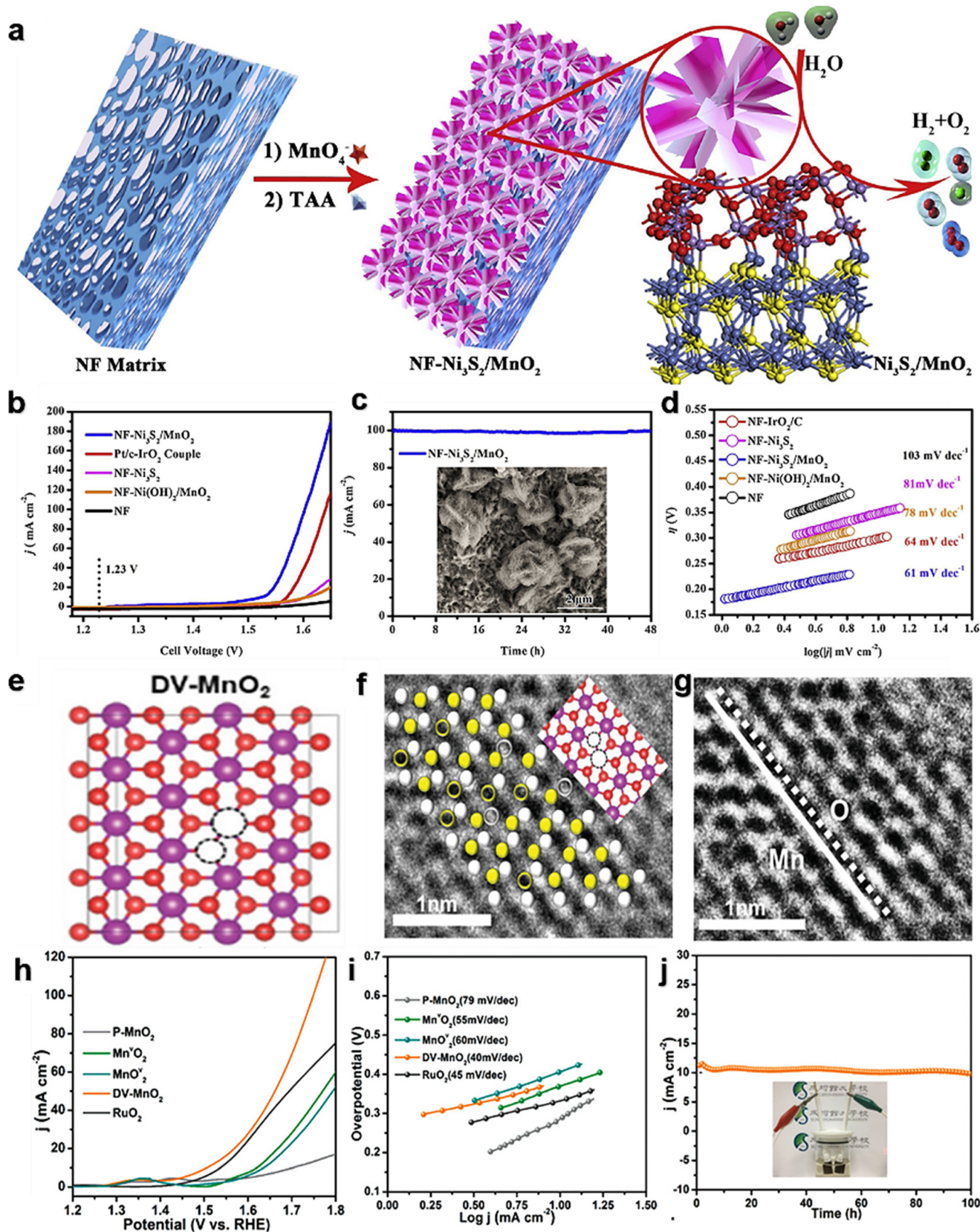
Fig. 8 (a) Schematic diagram of the NF–Ni$_3$S$_2$/MnO$_2$ catalyst synthesis process; (b) electrocatalytic OER performance of NF–Ni$_3$S$_2$/MnO$_2$; (c) chronopotentiometric response of NF–Ni$_3$S$_2$/MnO$_2$; (d) Tafel slopes of NF–Ni$_3$S$_2$/MnO$_2$. Reprinted with permission from ref. 101. Copyright 2019, *Appl. Catal., B*. (e) Local atomic configurations; (f) and (g) atomic-resolution STEM images of the (110) plane belonging to DV-MnO$_2$; (h) electrocatalytic OER performance of DV-MnO$_2$; (i) Tafel slopes of DV-MnO$_2$; (j) chronopotentiometric response of DV-MnO$_2$. Reprinted with permission from ref. 102. Copyright 2021, *Adv. Funct. Mater.*

(2) Controlling the formation of oxygen vacancies and improving the catalytic activity of the reaction.

Most non-noble metal oxides are inactive in acidic OER catalysis due to the high energy barrier and inherent slow kinetics of acidic OERs. Second, non-precious metals are more likely to lose catalytic activity in the high potential and acidic environment of PEM anodes. Therefore, the current research on non-noble metal doped manganese dioxide catalysts tends to be basic research. Research on manganese dioxide-doped non-precious metal catalysts has made great progress, but there are still some gaps compared with mature precious metal catalysts.

4 Application of manganese dioxide-based catalysts in PEM devices

Proton exchange membrane water electrolyzers (PEMWEs) are designed so that the OER and HER can occur in two separate compartments, applying the electric potential between the electrodes as the driving force so that high purity H_2 and O_2 can be collected. The basic design of a PEMWE cell is shown in Fig. 9a.[104] The OER and HER catalysts are coated on both sides of the PEM to form the membrane electrode assembly (MEA). The sulfonated tetrafluorovinyl fluoropolymer copolymer (Nafion) or perfluorosulfonic acid (PFSAs) is used as a binder and a proton-conducting phase in the anode and cathode catalyst layers. The MEA was usually compressed between the Ti-porous transport layer (PTL) on the anode side and the C-fiber gas diffusion layer (GDL) on the cathode side in order to promote water supply and gas product precipitation while maintaining electrical contact. The system is assembled and sealed by two bipolar plates (BPP) connected to an external water supply and product gas storage system.[105]
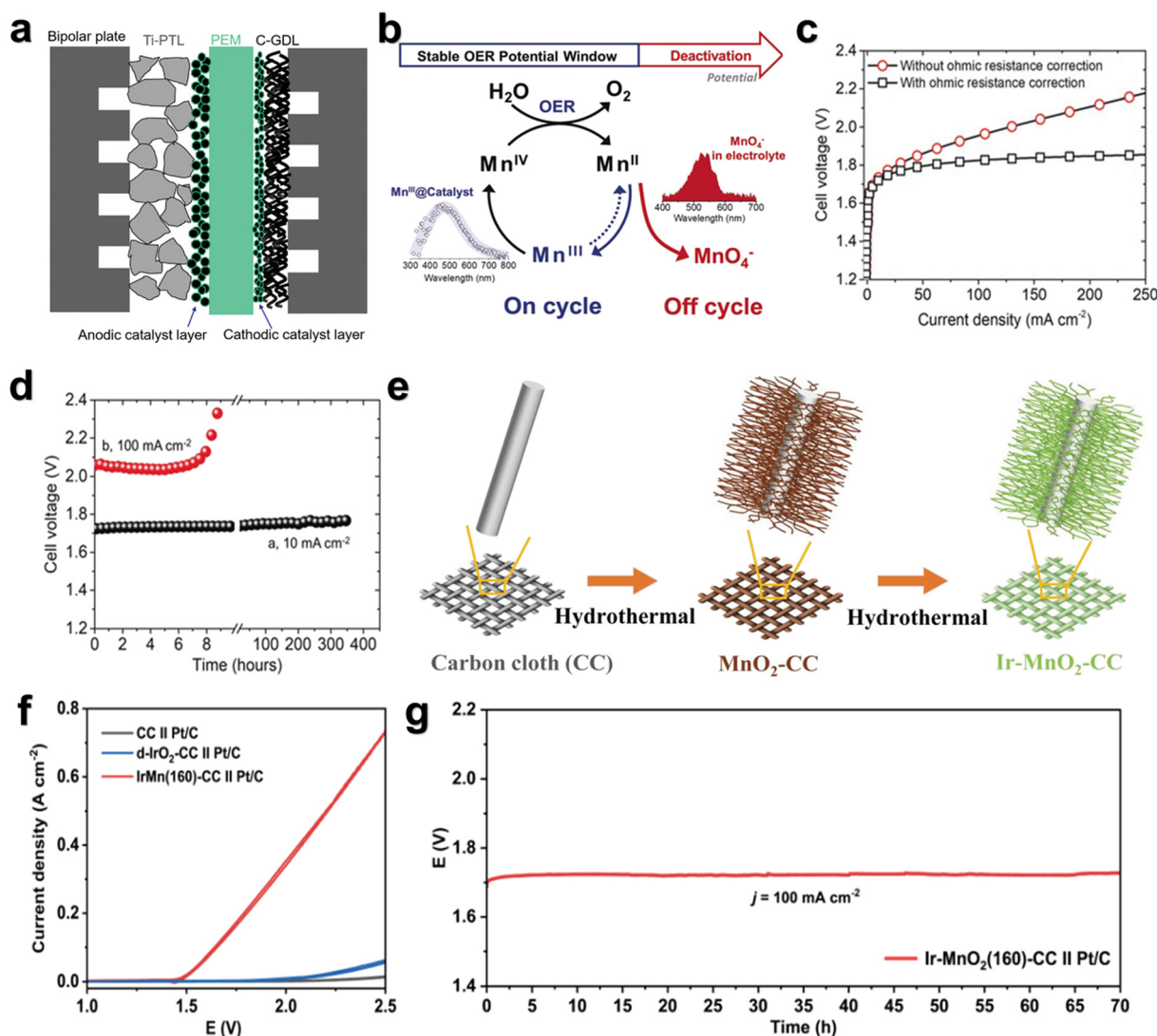
Fig. 9 (a) Schematic cross-section of a PEMWE single cell. Reprinted with permission from ref. 104. Copyright 2021, *Adv. Energy Mater.* (b) Window of opportunity. (c) Performance of γ-MnO₂ on carbon paper in a PEM setup. (d) Time dependence of the cell voltage at 10 mA cm⁻² and 100 mA cm⁻². Reprinted with permission from ref. 108. Copyright 2019, *Angew. Chem., Int. Ed.* (e) The synthesis procedure for the electrocatalyst Ir–MnO₂–CC. (f) The OER performance of catalysts tested in 0.5 M H₂SO₄ solution in PEMWE. (g) The stability of catalysts tested in 0.5 M H₂SO₄ solution in PEMWE. Reprinted with permission from ref. 109. Copyright 2023, *Adv. Sci.*

PEMWEs will play a key role in future sustainable hydrogen production.[106] Anodic catalysts in PEMWEs where critical oxygen evolution reactions occur require further improvement in performance and durability. At present, the main problem is how to inhibit degradation and reduce precious metal load. The main solution is to find a carrier with stable acid loading precious metal, so as to reduce the load content of precious metal under the premise of stability.[107] MnO_2 exhibits high conductivity and the required electrochemical stability in acidic media, so doping with some non-inert materials can alter the electronic structure and make it a potential anode catalyst for PEM electrolysis. In this section, the latest research progress of the application of manganese dioxide-based catalysts in PEM devices is reviewed.

Li et al.[108] reported that γ-MnO_2 can catalyze the OER at 10 mA cm^{-2} for over 8000 h in a pH = 2 electrolyte with no noticeable decrease in activity. In the PEM, the sum of cathode and anode overpotentials of MnO_2 at the current density of 10 mA cm^{-2} is about 480 mV (Fig. 9c) and only increases by 30 mV after 350 h operation at 10 mA cm^{-2} (Fig. 9d). It has also been demonstrated that the limitation on the stability of 3D metallic materials can be overcome by spectroscopic identification of the stable potential window, in which the OER can be catalyzed effectively while inhibiting the deactivation pathway (Fig. 9b). Weng et al.[109] reported a highly active and stable OER catalyst (Ir–MnO_2(160)–CC) (Fig. 9e). The overpotential under 10 mA cm^{-2} is only 181 mV (Fig. 9f) and the stability exceeds 180 h. In PEMWEs, Ir–MnO_2(160)–CC and Pt/C were applied as the anode and cathode, respectively. Ir–MnO_2(160)–CC//Pt/C could achieve a current density of 100 mA cm^{-2} at a small cell voltage of 1.65 V, and show negligible decay in 70 h (Fig. 9g), indicative of its potential for practical hydrogen production via PEMWE. It is proved that the formation of Mn–O–Ir coordination structure can optimize the adsorption strength of *OOH intermediates, thereby improving the activity and stability of the acidic OER. Although PEMWE testing with MnO_2-based catalysts is critical, there are very few studies that characterized their performance and durability in PEM devices. Therefore, future studies on MnO_2-based catalysts should try to put them in actual PEMWEs, which could truly move forward the MnO_2-based catalyst development.

The main challenge for PEMWEs is to improve the performance and reduce costs. Improving the power density and durability of the anode catalyst is a key factor in improving the performance of PEMWEs and reducing the cost. The anode catalyst must withstand not only the harsh acidic environment but also the high overvoltage, especially at high current density.[104] At present, the main solution is to find a carrier with stable acid loading precious metal, so as to reduce the load content of precious metal under the premise of stability. Among many transition metal base oxides, MnO_2 has unique acid resistance. Although MnO_2 itself has poor OER activity, it is a very suitable acidic OER catalyst carrier. Doping MnO_2 with OER-active precious metal elements can not only improve the stability and activity of

the catalyst, but also reduce the load of precious metal and thus reduce the cost. In recent years, although the development of non-noble metal based catalysts has increased rapidly, there is still a big gap compared with mature noble metal catalysts, especially in the acid OER where catalytic activity and stability problems still need to be solved. Therefore, in PEMWEs, manganese dioxide supported non-noble metal catalysts still have many problems, such as low activity and poor stability. In general, MnO_2 exhibits high conductivity and the required electrochemical stability in acidic media, so doping some non-inert materials can change the electronic structure and make it a potential anode catalyst for PEM electrolysis.

5 Conclusion and outlook

This paper reviews the basic understanding of the OER process catalyzed by manganese dioxide-based materials. The OER mechanisms, including the traditional adsorbent formation mechanism (AEM) and the emerging lattice oxygen oxidation mechanism (LOM), are discussed and the application of MnO_2-based catalysts in PEMWEs is summarized. Single manganese dioxide OER catalysts are reviewed in terms of crystal and morphology. Recent advances in the improvement of the OER catalytic performance of MnO_2-based catalysts using composite structures are reviewed.

Typically OER processes involve the conversion of transition metal-based catalysts to oxides at high electrical potentials, leading to valence transitions and structural disruption. Among the many transition metal-based catalysts, manganese oxides (MnO_x) have an abundance of valence states and crystal structures that exhibit excellent electrocatalytic performance in various electrochemical reactions, with MnO_2 showing unique catalytic activity and stability for the acidic OER, making MnO_2-based materials show unprecedented promise in the field of OER. α-MnO_2 and γ-MnO_2, which have a large tunnel structure and abundant defects in many different MnO_2 crystals, are more suitable as carriers of the OER catalyst. It is also very promising to improve the performance of MnO_2 based catalysts by morphological engineering. At present, manganese dioxide supported noble metal catalysts show exciting catalytic activity and catalytic stability in the acidic OER. By doping the precious metal with a single-atom, not only the utilization rate of the precious metal active site is improved, but also the load of precious metal and the cost is reduced, showing an unprecedented development prospect. Although manganese dioxide supported non-precious metal catalysts develop rapidly, there is still a big gap compared with mature precious metal catalysts. At present, manganese dioxide supported non-precious metal catalysts are commonly used in the alkaline OER, mainly because of the high reaction energy barrier in acidic medium. There is a strong synergistic effect between Ni and MnO_2, and the optimization of Ni-doped MnO_2 catalysts is very promising.

Manganese dioxide exhibits high conductivity and the required electrochemical stability in acidic media, so doping some non-inert materials can change the electronic structure and make it a potential anode catalyst for PEM electrolysis. Despite the exciting advances in MnO_2-based OER catalysts, their practical application to large-scale water electrolysis for hydrogen production is still in its early stages. Some of the current challenges and issues in the development of MnO_2-based catalysts are outlined below:

(1) The relationship between the crystal structure and catalytic performance of MnO_2 has not been fully elucidated, and the dynamic changes of MnO_2 phases and crystals during the OER process leading to the changes of catalytic performance are the main obstacles to investigate the relationship. The study of the correspondence between the crystal structure of MnO_2 and the catalytic performance for the OER is crucial for the rational design and synthesis of MnO_2-based catalysts with high catalytic activity and high stability.

(2) The control of crystal shape and morphology of MnO_2 in the loading process is still a problem to be solved. Cation insertion can significantly affect the layer spacing of MnO_2 and thus affect the catalytic activity of the OER. The effects of cations on the OER properties of MnO_2-based catalysts have not been studied systematically.

(3) Whether MnO_2-based catalysts doped with single-atoms are suitable for large-scale water electrolysis hydrogen production is still a question. Manganese dioxide exhibits high conductivity and the required electrochemical stability in acidic media, so doping some non-inert materials can change the electronic structure and make it a potential anode catalyst for PEM electrolysis. However, the application of single-atom doped MnO_2 catalysts in PEMs is still lacking.

(4) The lack of breakthrough in the field of acidic OER in manganese dioxide supported non-noble metal catalysts. The main reason is the high reactivity barrier of the OER in an acidic environment. Although manganese dioxide supported non-noble metal catalysts develop rapidly, there is still a big gap compared with mature noble metal catalysts, and there is still great development potential.

The basic strategies for optimizing MnO_2-based catalysts for the OER are summarized as follows.

(1) Controlling the crystal structure and morphology of MnO_2. Different crystalline forms of MnO_2 have different characteristics. It is preferred to select the appropriate MnO_2 with a tunnel structure, multiple defect edges and easy-to-fix active ions. The second is the morphology of MnO_2, which should have a large specific surface area, high quality diffusion efficiency and good conductivity. Selecting a suitable MnO_2 carrier with suitable crystal shape and morphology is critical to the performance of MnO_2-based catalysts.

(2) Selection of transition metal elements with synergistic effects with MnO_2 carriers. The direct synergistic effect between the conductive carrier and the active site can effectively improve the stability of the catalyst. The

preparation of composite electrode materials by doping precious metals and transition metal elements (Ti, Sb, Pb, Cu, Co, etc.) in MnO_2 is an effective way to improve the OER performance of MnO_2-based catalysts.

(3) The MnO_2 phase in the acid can be regenerated by the disambiguation reaction between Mn^{2+} and MnO^{4-}. Recapturing active sites in cation exchange reactions improves stability and has long-term implications.

Conflicts of interest

The authors declare no conflicts of interest.

Acknowledgements

References

1 X. Bai, L. Wang, B. Nan, T. Tang, X. Niu and J. Guan, Atomic manganese coordinated to nitrogen and sulfur for oxygen evolution, Nano Res., 2022, 15, 6019–6025.

2 K. Ham, J. Lee, K. Lee and J. Lee, Boosting the oxygen evolution reaction performance of wrinkled Mn(OH)2 via conductive activation with a carbon binder, J. Energy Chem., 2022, 71, 580–587.

3 C. Hu and L. Dai, Multifunctional carbon-Based metal-free electrocatalysts for simultaneous oxygen reduction, oxygen evolution, and hydrogen evolution, Adv. Mater., 2017, 29, 1604942.

4 Z.-H. Huang, Y. Song, D.-Y. Feng, Z. Sun, X. Sun and X.-X. Liu, High mass loading MnO_2 with hierarchical nanostructures for supercapacitors, ACS Nano, 2018, 12, 3557–3567.

5 W.-K. Han, J.-X. Wei, K. Xiao, T. Ouyang, X. Peng, S. Zhao and Z.-Q. Liu, Activating lattice oxygen in layered lithium oxides through cation vacancies for enhanced urea electrolysis, Angew. Chem., 2022, 61, e202206050.

6 G. Fu, X. Yan, Y. Chen, L. Xu, D. Sun, J.-M. Lee and Y. Tang, Boosting bifunctional oxygen electrocatalysis with 3D graphene aerogel-supported Ni/MnO particles, Adv. Mater., 2018, 30, 1704609.

7 K. Xiao, Y. Wang, P. Wu, L. Hou and Z.-Q. Liu, Activating lattice oxygen in spinel $ZnCo_2O_4$ through filling oxygen vacancies with fluorine for electrocatalytic oxygen evolution, Angew. Chem., 2023, 62, e202301408.

8 L. Zhang, J. Liang, L. Yue, K. Dong, J. Li, D. Zhao, Z. Li, S. Sun, Y. Luo, Q. Liu, G. Cui, A. Ali Alshehri, X. Guo and X. Sun, Benzoate anions-intercalated NiFe-layered double hydroxide nanosheet array with enhanced stability for

© 2023 The Author(s). Co-published by the Institute of Process Engineering, Chinese Academy of Sciences and the Royal Society of Chemistry

Ind. Chem. Mater., 2023, 1, 312–331 | 327

electrochemical seawater oxidation, *Nano Res. Energy*, 2022, **1**, e9120028.

9 K. Xiao, R.-T. Lin, J.-X. Wei, N. Li, H. Li, T. Ma and Z.-Q. Liu, Electrochemical disproportionation strategy to in-situ fill cation vacancies with Ru single atoms, *Nano Res.*, 2022, **15**, 4980–4985.

10 Y. Jia, L. Zhang, A. Du, G. Gao, J. Chen, X. Yan, C. L. Brown and X. Yao, Defect graphene as a trifunctional catalyst for electrochemical reactions, *Adv. Mater.*, 2016, **28**, 9532–9538.

11 Y. Luo, Z. Zhang, M. Chhowalla and B. Liu, Recent advances in design of electrocatalysts for high-current-density water splitting, *Adv. Mater.*, 2022, **34**, e2108133.

12 S. Gupta, S. Zhao, X. X. Wang, S. Hwang, S. Karakalos, S. V. Devaguptapu, S. Mukherjee, D. Su, H. Xu and G. Wu, Quaternary FeCoNiMn-based nanocarbon electrocatalysts for bifunctional oxygen reduction and evolution: promotional role of Mn doping in stabilizing carbon, *ACS Catal.*, 2017, **7**, 8386–8393.

13 D. Jeong, K. Jin, S. E. Jerng, H. Seo, D. Kim, S. H. Nahm, S. H. Kim and K. T. Nam, Mn_5O_8 nanoparticles as efficient water oxidation catalysts at neutral pH, *ACS Catal.*, 2015, **5**, 4624–4628.

14 J. Wei, K. Xiao, Y. Chen, X.-P. Guo, B. Huang and Z.-Q. Liu, In situ precise anchoring of Pt single atoms in spinel Mn_3O_4 for a highly efficient hydrogen evolution reaction, *Energy Environ. Sci.*, 2022, **15**, 4592–4600.

15 F. Gao, J. He, H. Wang, J. Lin, R. Chen, K. Yi, F. Huang, Z. Lin and M. Wang, Te-mediated electro-driven oxygen evolution reaction, *Nano Res. Energy*, 2022, **1**, e9120029.

16 H. Jing, P. Zhu, X. Zheng, Z. Zhang, D. Wang and Y. Li, Theory-oriented screening and discovery of advanced energy transformation materials in electrocatalysis, *Adv. Powder Mater.*, 2022, **1**, 100013.

17 S. Niu, X.-P. Kong, S. Li, Y. Zhang, J. Wu, W. Zhao and P. Xu, Low Ru loading $RuO_2/(Co,Mn)_3O_4$ nanocomposite with modulated electronic structure for efficient oxygen evolution reaction in acid, *Appl. Catal., B*, 2021, **297**, 120442.

18 S. Jo, W. B. Park, K. B. Lee, H. Choi, K.-S. Lee, D. Ahn, Y.-W. Lee, K.-S. Sohn, J. Hong and J. I. Sohn, Bi/BiFe(oxy)hydroxide for sustainable lattice oxygen-boosted electrocatalysis at a practical high current density, *Appl. Catal., B*, 2022, **317**, 121685.

19 C. Wang, A. Schechter and L. Feng, Iridium-based catalysts for oxygen evolution reaction in acidic media: Mechanism, catalytic promotion effects and recent progress, *Nano Res. Energy*, 2023, **2**, e9120056.

20 Y. Li, T. Wang, M. Asim, L. Pan, R. Zhang, Z.-F. Huang, Z. Chen, C. Shi, X. Zhang and J.-J. Zou, Manipulating spin polarization of defected Co_3O_4 for highly efficient electrocatalysis, *Trans. Tianjin Univ.*, 2022, **28**, 163–173.

21 X. Peng, Y. Guo, Q. Yin, J. Wu, J. Zhao, C. Wang, S. Tao, W. Chu, C. Wu and Y. Xie, Double-exchange effect in two-dimensional MnO_2 nanomaterials, *J. Am. Chem. Soc.*, 2017, **139**, 5242–5248.

22 H. Gu, X. Liu, X. Liu, C. Ling, K. Wei, G. Zhan, Y. Guo and L. Zhang, Adjacent single-atom irons boosting molecular oxygen activation on MnO_2, *Nat. Commun.*, 2021, **12**, 5422.

23 D. Li, H. Baydoun, B. Kulikowski and S. L. Brock, Boosting the catalytic performance of iron phosphide nanorods for the oxygen evolution reaction by incorporation of manganese, *Chem. Mater.*, 2017, **29**, 3048–3054.

24 C. Zhang, X. Zhan, T. Al-Zoubi, Y. Ma, P.-C. Shih, F. Wang, W. Chen, S. Pidaparthy, R. M. Stephens, Q. Chen, J.-M. Zuo and H. Yang, Electrochemical generation of birnessite MnO_2 nanoflowers for intercalation of Mg^{2+} ions, *Nano Energy*, 2022, **102**, 107696.

25 L. Li, X. Cao, J. Huo, J. Qu, W. Chen, C. Liu, Y. Zhao, H. Liu and G. Wang, High valence metals engineering strategies of Fe/Co/Ni-based catalysts for boosted OER electrocatalysis, *J. Energy Chem.*, 2023, **76**, 195–213.

26 Y. Du, B. Li, G. Xu and L. Wang, Recent advances in interface engineering strategy for highly-efficient electrocatalytic water splitting, *InfoMat*, 2023, **5**, e12377.

27 L.-H. Liu, N. Li, M. Han, J.-R. Han and H.-Y. Liang, Scalable synthesis of nanoporous high entropy alloys for electrocatalytic oxygen evolution, *Rare Met.*, 2022, **41**, 125–131.

28 J. Shang, B. Xie, Y. Li, X. Wei, N. Du, H. Li, W. Hou and R. Zhang, Inflating strategy to form ultrathin hollow MnO_2 nanoballoons, *ACS Nano*, 2016, **10**, 5916–5921.

29 L. Tang, L. Fan, Z. Chen, J. Tian, H. Guo, M. Peng, F. Zuo, X. Fu, M. Li, Y. Bu, J. Luo, J. Li and Y. Sun, Binary-dopant promoted lattice oxygen participation in OER on cobaltate electrocatalyst, *Chem. Eng. J.*, 2021, **417**, 129324.

30 Y. Zhou, F. Chen, R. Tian, S. Huang, R. Chen, M. Li, T. Wan, Z. Han, D. Wang and D. Chu, Oxygen vacancies and band gap engineering of vertically aligned MnO_2 porous nanosheets for efficient oxygen evolution reaction, *Surf. Interfaces*, 2021, **26**, 101398.

31 J. Qi, H. Liu, H. Xu, L. Hu, C. Wang, Y. Zhang, M. Feng and W. Lü, Surface atomic decoration of a manganite to a modulable oxygen evolution reaction, *ACS Appl. Mater. Interfaces*, 2021, **13**, 61267–61274.

32 W.-Y. Fu, Y.-X. Lin, M.-S. Wang, S. Si, L. Wei, X.-S. Zhao and Y.-S. Wei, Sepaktakraw-like catalyst Mn-doped CoP enabling ultrastable electrocatalytic oxygen evolution at 100 mA·cm^{-2} in alkali media, *Rare Met.*, 2022, **41**, 3069–3077.

33 M. Yang, C. H. Zhang, N. W. Li, D. Luan, L. Yu and X. W. D. Lou, Design and synthesis of hollow nanostructures for electrochemical water splitting, *Adv. Sci.*, 2022, **9**, e2105135.

34 X. Yuan, Z. Ma, S. Jian, H. Ma, Y. Lai, S. Deng, X. Tian, C.-P. Wong, F. Xia and Y. Dong, Mesoporous nitrogen-doped carbon MnO_2 multichannel nanotubes with high performance for Li-ion batteries, *Nano Energy*, 2022, **97**, 107235.

35 J. H. Siow, M. R. Bilad, W. Caesarendra, J. J. Leam, M. A. Bustam, N. S. Sambudi, Y. Wibisono and T. M. Mahlia, Progress in development of nanostructured manganese oxide as catalyst for oxygen reduction and evolution reaction, *Energies*, 2021, **14**, 6385.

36 K. Zhang, X. Liang, L. Wang, K. Sun, Y. Wang, Z. Xie, Q. Wu, X. Bai, M. S. Hamdy, H. Chen and X. Zou, Status and perspectives of key materials for PEM electrolyzer, *Nano Res. Energy*, 2022, **1**, e9120032.

37 M. You, X. Du, X. Hou, Z. Wang, Y. Zhou, H. Ji, L. Zhang, Z. Zhang, S. Yi and D. Chen, In-situ growth of ruthenium-based nanostructure on carbon cloth for superior electrocatalytic activity towards HER and OER, *Appl. Catal., B*, 2022, **317**, 121729.

38 N. Xu, Q. Nie, L. Luo, C. Yao, Q. Gong, Y. Liu, X.-D. Zhou and J. Qiao, Controllable hortensia-like MnO_2 synergized with carbon nanotubes as an efficient electrocatalyst for long-term metal–air batteries, *ACS Appl. Mater. Interfaces*, 2019, **11**, 578–587.

39 Z. Li, X. Wu, X. Jiang, B. Shen, Z. Teng, D. Sun, G. Fu and Y. Tang, Surface carbon layer controllable Ni_3Fe particles confined in hierarchical N-doped carbon framework boosting oxygen evolution reaction, *Adv. Powder Mater.*, 2022, **1**, 100020.

40 H. Cui, H.-X. Liao, Z.-L. Wang, J.-P. Xie, P.-F. Tan, D.-W. Chu and P. Jun, Synergistic electronic interaction between ruthenium and nickel-iron hydroxide for enhanced oxygen evolution reaction, *Rare Met.*, 2022, **41**, 2606–2615.

41 K. Zeng, W. Li, Y. Zhou, Z. Sun, C. Lu, J. Yan, J.-H. Choi and R. Yang, Multilayer hollow $MnCo_2O_4$ microsphere with oxygen vacancies as efficient electrocatalyst for oxygen evolution reaction, *Chem. Eng. J.*, 2021, **421**, 127831.

42 Y. Zhao, J. Zhang, W. Wu, X. Guo, P. Xiong, H. Liu and G. Wang, Cobalt-doped MnO_2 ultrathin nanosheets with abundant oxygen vacancies supported on functionalized carbon nanofibers for efficient oxygen evolution, *Nano Energy*, 2018, **54**, 129–137.

43 F. Wang, H. Zhao, Y. Ma, Y. Yang, B. Li, Y. Cui, Z. Guo and L. Wang, Core-shell-structured $Co@Co_4N$ nanoparticles encapsulated into MnO-modified porous N-doping carbon nanocubes as bifunctional catalysts for rechargeable Zn–air batteries, *J. Energy Chem.*, 2020, **50**, 52–62.

44 Z. Ye, T. Li, G. Ma, Y. Dong and X. Zhou, Metal-ion (Fe, V, Co, and Ni)-doped MnO_2 ultrathin nanosheets supported on carbon fiber paper for the oxygen evolution reaction, *Adv. Funct. Mater.*, 2017, **27**, 1704083.

45 Y. Zhang, B. Ouyang, G. Long, H. Tan, Z. Wang, Z. Zhang, W. Gao, R. S. Rawat and H. J. Fan, Enhancing bifunctionality of CoN nanowires by Mn doping for long-lasting Zn-air batteries, *Sci. China: Chem.*, 2020, **63**, 890–896.

46 X. Zhao, X. Li, Y. Yan, Y. Xing, S. Lu, L. Zhao, S. Zhou, Z. Peng and J. Zeng, Electrical and structural engineering of cobalt selenide nanosheets by Mn modulation for efficient oxygen evolution, *Appl. Catal., B*, 2018, **236**, 569–575.

47 K. Wu, C. Cao, K. Li, C. Lyu, J. Cheng, H. Li, P. Hu, J. Wu, W.-M. Lau, X. Zhu, P. Qian and J. Zheng, Regulating electronic structure by Mn doping for nickel cobalt hydroxide nanosheets/carbon nanotube to promote oxygen evolution reaction and oxidation of urea and hydrazine, *Chem. Eng. J.*, 2023, **452**, 139527.

48 S. Yan, Y. Xue, S. Li, G. Shao and Z. Liu, Enhanced Bifunctional Catalytic Activity of manganese oxide/perovskite hierarchical core–shell materials by adjusting the interface for metal–air batteries, *ACS Appl. Mater. Interfaces*, 2019, **11**, 25870–25881.

49 K. Zhang and R. Zou, Advanced Transition Metal-Based OER Electrocatalysts: Current Status, Opportunities, and Challenges, *Small*, 2021, **17**, e2100129.

50 N. V. Bôas, J. B. Souza Jr, L. C. Varanda, S. A. S. Machado and M. L. Calegaro, Bismuth and cerium doped cryptomelane-type manganese dioxide nanorods as bifunctional catalysts for rechargeable alkaline metal-air batteries, *Appl. Catal., B*, 2019, **258**, 118014.

51 Y. Tang, S. Zheng, S. Cao, H. Xue and H. Pang, Advances in the application of manganese dioxide and its composites as electrocatalysts for the oxygen evolution reaction, *J. Mater. Chem. A*, 2020, **8**, 18492–18514.

52 Ö. N. Avcı, L. Sementa and A. Fortunelli, Mechanisms of the oxygen evolution reaction on $NiFe_2O_4$ and $CoFe_2O_4$ Inverse-Spinel Oxides, *ACS Catal.*, 2022, **12**, 9058–9073.

53 J. Hu, D. Jiang, Z. Weng, Y. Pan, Z. Li, H. Du and Y. Yuan, A universal electrochemical activation enabling lattice oxygen activation in nickel-based catalyst for efficient water oxidation, *Chem. Eng. J.*, 2022, **430**, 132736.

54 M. Yin, H. Miao, R. Hu, Z. Sun and H. Li, Manganese dioxides for oxygen electrocatalysis in energy conversion and storage systems over full pH range, *J. Power Sources*, 2021, **494**, 229779.

55 J. Li, L. Zheng, B. Huang, Y. Hu, L. An, Y. Yao, M. Lu, J. Jin, N. Zhang, P. Xi and C.-H. Yan, Activated Ni–O–Ir enhanced electron transfer for boosting oxygen evolution reaction activity of $LaNi_{1-x}Ir_xO_3$, *Small*, 2022, 2204723.

56 H.-Y. Qu, X. He, Y. Wang and S. Hou, Electrocatalysis for the oxygen evolution reaction in acidic media: progress and challenges, *Appl. Sci.*, 2021, **11**, 4320.

57 C. Gao, L. Liu, T. Yu and F. Yang, Development of a novel carbon-based conductive membrane with in-situ formed MnO_2 catalyst for wastewater treatment in bio-electrochemical system (BES), *J. Membr. Sci.*, 2018, **549**, 533–542.

58 M. Lu, Y. Zheng, Y. Hu, B. Huang, D. Ji, M. Sun, J. Li, Y. Peng, R. Si, P. Xi and C.-H. Yan, Artificially steering electrocatalytic oxygen evolution reaction mechanism by regulating oxygen defect contents in perovskites, *Sci. Adv.*, 2022, **8**, eabq3563.

59 Y. Zhou, Z. Zhou, L. Hu, R. Tian, Y. Wang, H. Arandiyan, F. Chen, M. Li, T. Wan, Z. Han, Z. Ma, X. Lu, C. Cazorla, T. Wu and D. Chu, A facile approach to tailor electrocatalytic properties of MnO_2 through tuning phase transition, surface morphology and band structure, *Chem. Eng. J.*, 2022, **438**, 135561.

60 H. Zhang, Y. Gao, H. Xu, D. Guan, Z. Hu, C. Jing, Y. Sha, Y. Gu, Y. C. Huang, Y. C. Chang, C. W. Pao, X. Xu, J. F. Lee, Y. Y. Chin, H. J. Lin, C. T. Chen, Y. Chen, Y. Guo, M. Ni, W. Zhou and Z. Shao, Combined corner-sharing and edge-sharing networks in hybrid nanocomposite with unusual

© 2023 The Author(s). Co-published by the Institute of Process Engineering, Chinese Academy of Sciences and the Royal Society of Chemistry

Ind. Chem. Mater., 2023, **1**, 312–331 | 329

lattice-oxygen activation for efficient water oxidation, *Adv. Funct. Mater.*, 2022, **32**, 2207618.

61 Y. Ma, Y. An, Z. Xu, L. Cheng and W. Yuan, Activating lattice oxygen of two-dimensional $Mn_{Xn-1}O_2$ MXenes via zero-dimensional graphene quantum dots for water oxidation, *Sci. China Mater.*, 2022, **65**, 3053–3061.

62 Z. M. Chan, D. A. Kitchaev, J. N. Weker, C. Schnedermann, K. Lim, G. Ceder, W. Tumas, M. F. Toney and D. G. Nocera, Electrochemical trapping of metastable Mn^{3+} ions for activation of MnO_2 oxygen evolution catalysts, *Proc. Natl. Acad. Sci. U. S. A.*, 2018, **115**, E5261–E5268.

63 Q. Qin, H. Jang, Y. Wang, L. Zhang, Z. Li, M. G. Kim, S. Liu, X. Liu and J. Cho, Gettering la effect from La_3IrO_7 as a highly efficient electrocatalyst for oxygen evolution reaction in acid media, *Adv. Energy Mater.*, 2021, **11**, 2003561.

64 Y. Zhao, J. Hu, C.-L. Chiang, Y. Li, W. Yang, Z. Yang, W.-H. Hung, Y.-G. Lin, Z. Chen, B. Li, P. Gao and H. Li, Ruthenium oxychloride supported by manganese oxide for stable oxygen evolution in acidic media, *J. Mater. Chem. A*, 2022, **10**, 20964–20974.

65 A. Zagalskaya and V. Alexandrov, Role of defects in the interplay between adsorbate evolving and lattice oxygen mechanisms of the oxygen evolution reaction in RuO_2 and IrO_2, *ACS Catal.*, 2020, **10**, 3650–3657.

66 L. Bigiani, D. Barreca, A. Gasparotto, T. Andreu, J. Verbeeck, C. Sada, E. Modin, O. I. Lebedev, J. R. Morante and C. Maccato, Selective anodes for seawater splitting via functionalization of manganese oxides by a plasma-assisted process, *Appl. Catal., B*, 2021, **284**, 119684.

67 X. Wang, H. Zhong, S. Xi, W. S. V. Lee and J. Xue, Understanding of oxygen redox in the oxygen evolution reaction, *Adv. Mater.*, 2022, e2107956.

68 T. Xia, C. Liu, Y. Lu, W. Jiang, H. Li, Y. Ma, Y. Wu and G. Che, Regulating Ru-based double perovskite against lattice oxygen oxidation by incorporating Ir for efficient and stable acidic oxygen evolution reaction, *Appl. Surf. Sci.*, 2022, **605**, 154727.

69 J. S. Yoo, X. Rong, Y. Liu and A. M. Kolpak, Role of lattice oxygen participation in understanding trends in the oxygen evolution reaction on perovskites, *ACS Catal.*, 2018, **8**, 4628–4636.

70 O. Icten, D. Ozer and G. Elmaci, Boron doped cryptomelane as a highly efficient electrocatalyst for the oxygen evolution reaction, *Int. J. Hydrogen Energy*, 2021, **46**, 39810–39821.

71 X. Xu, Y. Pan, Y. Zhong, C. Shi, D. Guan, L. Ge, Z. Hu, Y. Y. Chin, H. J. Lin, C. T. Chen, H. Wang, S. P. Jiang and Z. Shao, New undisputed evidence and strategy for enhanced lattice-oxygen participation of perovskite electrocatalyst through cation deficiency manipulation, *Adv. Sci.*, 2022, **9**, e2200530.

72 A. Roy, A. Ray, S. Saha, M. Ghosh, T. Das, M. Nandi, G. Lal and S. Das, Influence of electrochemical active surface area on the oxygen evolution reaction and energy storage performance of MnO_2-multiwalled carbon nanotube composite, *Int. J. Energy Res.*, 2021, **45**, 16908–16921.

73 J. Lu, H. Wang, Y. Sun, X. Wang, X. Song and R. Wang, Charge state manipulation induced through cation intercalation into MnO_2 sheet arrays for efficient water splitting, *Chem. Eng. J.*, 2021, **417**, 127894.

74 H. Feizi, S. M. Hosseini, Z. Zand and M. M. Najafpour, Electrochemical induction of Mn(III) in the structure of Mn(IV) oxide: Toward a new approach for water splitting, *Int. J. Hydrogen Energy*, 2022, **47**, 7813–7822.

75 S. Wan, Y. Li, L. Xu, W. Zhang and R. Cao, Autologous Mn oxides as electrocatalysts to identify the origin of the water oxidation activity, *Mater. Today Sustain.*, 2022, **17**, 100106.

76 M. Guo, Z. Wei and Q. Zhang, Electrochemical construction of S-doped MnO_x/Mn integrated film on carbon paper in a choline chloride based deep eutectic solvent for enhanced electrochemical water oxidation, *Int. J. Hydrogen Energy*, 2022, **47**, 6029–6043.

77 K. Bera, A. Karmakar, K. Karthick, S. S. Sankar, S. Kumaravel, R. Madhu and S. Kundu, Enhancement of the OER kinetics of the less-explored α-MnO_2 via nickel doping approaches in alkaline medium, *Inorg. Chem.*, 2021, **60**, 19429–19439.

78 J. Heese-Gärtlein, A. Rabe and M. Behrens, Challenges in the application of manganese oxide powders as OER Electrocatalysts: Synthesis, Characterization, Activity and Stability of Nine Different Mn_xO_y Compounds, *Z. Anorg. Allg. Chem.*, 2021, **647**, 1363–1372.

79 G. M. S. Salvador, A. L. Silva, L. P. C. Silva, F. B. Passos and N. M. F. Carvalho, Enhanced activity of Pd/α-MnO_2 for electrocatalytic oxygen evolution reaction, *Int. J. Hydrogen Energy*, 2021, **46**, 26976–26988.

80 S. Pakseresht, T. Cetinkaya, A. W. M. Al-Ogaili and H. Akbulut, Urchin-like core-shell TiO_2/α-MnO_2 nanostructures as an active catalyst for rechargeable lithium-oxygen battery, *Adv. Powder Technol.*, 2021, **32**, 895–907.

81 A. Gowrisankar and S. Thangavelu, Effect of β-MnO_2 on controlled polymorphism of $VO_2(x)$ (x = A, B, M polymorphs) microstructures anchored on two-dimensional reduced graphene oxide nanosheets for overall water splitting, *J. Phys. Chem. C*, 2022, **126**, 3419–3431.

82 W. Ye, F. Xu, L. Jiang, N. Duan, J. Li, F. Zhang, G. Zhang and L. Chen, A novel functional lead-based anode for efficient lead dissolution inhibition and slime generation reduction in zinc electrowinning, *J. Cleaner Prod.*, 2021, **284**, 124767.

83 H. Kakizaki, H. Ooka, T. Hayashi, A. Yamaguchi, N. Bonnet-Mercier, K. Hashimoto and R. Nakamura, Evidence that crystal facet orientation dictates oxygen evolution intermediates on rutile manganese oxide, *Adv. Funct. Mater.*, 2018, **28**, 1706319.

84 Y.-F. Li and Z.-P. Liu, Active site revealed for water oxidation on electrochemically induced δ-MnO_2: role of spinel-to-layer phase transition, *J. Am. Chem. Soc.*, 2018, **140**, 1783–1792.

85 G. Yan, Y. Lian, Y. Gu, C. Yang, H. Sun, Q. Mu, Q. Li, W. Zhu, X. Zheng, M. Chen, J. Zhu, Z. Deng and Y. Peng, Phase and morphology transformation of MnO_2 induced by ionic liquids toward efficient water oxidation, *ACS Catal.*, 2018, **8**, 10137–10147.

86 Y. Chen, S. Yang, H. Liu, W. Zhang and R. Cao, An unusual network of α-MnO₂ nanowires with structure-induced hydrophilicity and conductivity for improved electrocatalysis, *Chin. J. Catal.*, 2021, **42**, 1724–1731.

87 Y. Qin, Y. Liu, Y. Zhang, Y. Gu, Y. Lian, Y. Su, J. Hu, X. Zhao, Y. Peng, K. Feng, J. Zhong, M. H. Rummeli and Z. Deng, Ru-substituted MnO₂ for accelerated water oxidation: the feedback of strain-induced and polymorph-dependent structural changes to the catalytic activity and mechanism, *ACS Catal.*, 2023, **13**, 256–266.

88 S. D. Ghadge, P. P. Patel, M. K. Datta, O. I. Velikokhatnyi, R. Kuruba, P. M. Shanthi and P. N. Kumta, Fluorine substituted (Mn,Ir)O₂:F high performance solid solution oxygen evolution reaction electro-catalysts for PEM water electrolysis, *RSC Adv.*, 2017, **7**, 17311–17324.

89 C. Lin, J.-L. Li, X. Li, S. Yang, W. Luo, Y. Zhang, S.-H. Kim, D.-H. Kim, S. S. Shinde, Y.-F. Li, Z.-P. Liu, Z. Jiang and J.-H. Lee, In-situ reconstructed Ru atom array on α-MnO₂ with enhanced performance for acidic water oxidation, *Nat. Catal.*, 2021, **4**, 1012–1023.

90 Z. Shi, Y. Wang, J. Li, X. Wang, Y. Wang, Y. Li, W. Xu, Z. Jiang, C. Liu, W. Xing and J. Ge, Confined Ir single sites with triggered lattice oxygen redox: Toward boosted and sustained water oxidation catalysis, *Joule*, 2021, **5**, 2164–2176.

91 K. Xiao, R.-T. Lin, J.-X. Wei, N. Li, H. Li, T. Ma and Z.-Q. Liu, Electrochemical disproportionation strategy to in-situ fill cation vacancies with Ru single atoms, *Nano Res.*, 2022, **15**, 4980–4985.

92 M. Sookhakian, H. Ullah, M. A. M. Teridi, G. B. Tong, W. J. Basirun and Y. Alias, Boron-doped graphene-supported manganese oxide nanotubes as an efficient non-metal catalyst for the oxygen reduction reaction, Sustainable, *Energy Fuels*, 2020, **4**, 737–749.

93 Y. Guo, M. Wang, Q. Zhu, D. Xiao and D. Ma, Ensemble effect for single-atom, small cluster and nanoparticle catalysts, *Nat. Catal.*, 2022, **5**, 766–776.

94 J.-W. Lee, S. Seo, P. Nandi, H. S. Jung, N.-G. Park and H. Shin, Dynamic structural property of organic-inorganic metal halide perovskite, *iScience*, 2021, **24**, 101959.

95 A. M. Harzandi, S. Shadman, A. S. Nissimagoudar, D. Y. Kim, H.-D. Lim, J. H. Lee, M. G. Kim, H. Y. Jeong, Y. Kim and K. S. Kim, Ruthenium core–shell engineering with nickel single atoms for selective oxygen evolution via nondestructive mechanism, *Adv. Energy Mater.*, 2021, **11**, 2003448.

96 H. Liao, X. Guo, Y. Hou, H. Liang, Z. Zhou and H. Yang, Construction of defect-rich Ni-Fe-Doped K(0.23) MnO(2) cubic nanoflowers via etching prussian blue analogue for efficient overall water splitting, *Small*, 2020, **16**, e1905223.

97 J. N. Heo, J. Shin, T. Yoon, N. Son and M. Kang, Effective alkaline water electrolysis on nwMnO₂-nsNi(OH)₂ composite electrode via lattice oxygen participant adsorbate evolving mechanism, *Appl. Surf. Sci.*, 2021, **567**, 150281.

98 Y. Yang, X. Su, L. Zhang, P. Kerns, L. Achola, V. Hayes, R. Quardokus, S. L. Suib and J. He, Intercalating MnO₂ nanosheets with transition metal cations to enhance oxygen evolution, *ChemCatChem*, 2019, **11**, 1689–1700.

99 H. Zhang, Y. Jia, Y. Li, L. Wang, C. Ouyang and S. Zhong, Ni/Ce co-doping δ-MnO₂ nanosheets with oxygen vacancy for enhanced electrocatalytic oxygen evolution reaction, *Int. J. Hydrogen Energy*, 2022, **48**, 2652–2662.

100 X. Zhang, Z. Song, Q. Yan, W. Cong, L. Yang, K. Zhu, K. Ye, J. Yan, D. Cao and G. Wang, Tremella-like manganese dioxide complex (Fe,Ni)₃S₄ hybrid catalyst for highly efficient oxygen evolution reaction, *J. Power Sources*, 2021, **515**, 230627.

101 Y. Xiong, L. Xu, C. Jin and Q. Sun, Interface-engineered atomically thin Ni₃S₂/MnO₂ heterogeneous nanoarrays for efficient overall water splitting in alkaline media, *Appl. Catal., B*, 2019, **254**, 329–338.

102 Y. Liu, H. T. D. Bui, A. R. Jadhav, T. Yang, S. Saqlain, Y. Luo, J. Yu, A. Kumar, H. Wang, L. Wang, V. Q. Bui, M. G. Kim, Y. D. Kim and H. Lee, Revealing the synergy of cation and anion vacancies on improving overall water splitting kinetics, *Adv. Funct. Mater.*, 2021, **31**, 2010718.

103 Y. Niu, X. Teng, S. Gong, X. Liu, M. Xu and Z. Chen, Boosting oxygen electrocatalysis for flexible zinc-air batteries by interfacing iron group metals and manganese oxide in porous carbon nanowires, *Energy Stor. Mater.*, 2021, **43**, 42–52.

104 C. V. Pham, D. Escalera-López, K. Mayrhofer, S. Cherevko and S. Thiele, Essentials of high performance water electrolyzers – from catalyst layer materials to electrode engineering, *Adv. Energy Mater.*, 2021, **11**, 2101998.

105 M. Carmo, D. L. Fritz, J. Mergel and D. Stolten, A comprehensive review on PEM water electrolysis, *Int. J. Hydrogen Energy*, 2013, **38**, 4901–4934.

106 Q. Feng, X. Z. Yuan, G. Liu, B. Wei, Z. Zhang, H. Li and H. Wang, A review of proton exchange membrane water electrolysis on degradation mechanisms and mitigation strategies, *J. Power Sources*, 2017, **366**, 33–55.

107 K. Kadakia, M. K. Datta, O. I. Velikokhatnyi, P. Jampani, S. K. Park, S. J. Chung and P. N. Kumta, High performance fluorine doped (Sn,Ru)O₂ oxygen evolution reaction electro-catalysts for proton exchange membrane based water electrolysis, *J. Power Sources*, 2014, **245**, 362–370.

108 A. Li, H. Ooka, N. Bonnet, T. Hayashi, Y. Sun, Q. Jiang, C. Li, H. Han and R. Nakamura, Stable potential windows for long-term electrocatalysis by manganese oxides under acidic conditions, *Angew. Chem., Int. Ed.*, 2019, **58**, 5054–5058.

109 Y. Weng, K. Wang, S. Li, Y. Wang, L. Lei, L. Zhuang and Z. Xu, High-valence-manganese driven strong anchoring of iridium species for robust acidic water oxidation, *Adv. Sci.*, 2023, **10**, 2205920.

110 Y. Tang, S. Zheng, Y. Xu, X. Xiao, H. Xue and H. Pang, Advanced batteries based on manganese dioxide and its composites, *Energy Stor. Mater.*, 2018, **12**, 284–309.

© 2023 The Author(s). Co-published by the Institute of Process Engineering, Chinese Academy of Sciences and the Royal Society of Chemistry

Ind. Chem. Mater., 2023, **1**, 312–331 | **331**